GROWTH OF SEMI-POLAR (11-22) GaN EPITAXIAL LAYER ON M-PLANE SAPPHIRE VIA MOCVD

MOHD AFIQ BIN ANUAR

FACULTY OF SCIENCE
UNIVERSITI MALAYA
KUALA LUMPUR

2020

GROWTH OF SEMI-POLAR (11-22) GaN EPITAXIAL LAYER ON M-PLANE SAPPHIRE VIA MOCVD

MOHD AFIQ BIN ANUAR

DISSERTATION SUBMITTED IN FULLFILLMENT OF
THE REQUIREMENT FOR THE DEGREE OF
MASTER OF SCIENCE

DEPARTMENT OF PHYSICS
FACULTY OF SCIENCE
UNIVERSITI MALAYA
KUALA LUMPUR

2020

UNIVERSITI MALAYA
ORIGINAL LITERARY WORK DECLARATION

Name of Candidate: **MOHD AFIQ BIN ANUAR**

Matric No: **SMA 180005**

Name of Degree: **MASTER OF SCIENCE**

Title of Project Paper/Research Report/Dissertation/Thesis (“this Work”):

GROWTH OF SEMI-POLAR (11-22) GaN ON M-PLANE SAPPHIRE VIA MOCVD

Field of Study:

EXPERIMENTAL PHYSICS

I do solemnly and sincerely declare that:

(1) I am the sole author/writer of this Work;
(2) This Work is original;
(3) Any use of any work in which copyright exists was done by way of fair dealing and for permitted purposes and any excerpt or extract from, or reference to or reproduction of any copyright work has been disclosed expressly and sufficiently and the title of the Work and its authorship have been acknowledged in this Work;
(4) I do not have any actual knowledge nor do I ought reasonably to know that the making of this work constitutes an infringement of any copyright work;
(5) I hereby assign all and every rights in the copyright to this Work to the University of Malaya (“UM”), who henceforth shall be owner of the copyright in this Work and that any reproduction or use in any form or by any means whatsoever is prohibited without the written consent of UM having been first had and obtained;
(6) I am fully aware that if in the course of making this Work I have infringed any copyright whether intentionally or otherwise, I may be subject to legal action or any other action as may be determined by UM

Candidate’s Signature Date:

Subscribed and solemnly declared before,

Witness’s Signature Date:

Name:

Designation:

GROWTH OF SEMI-POLAR (11-22) GaN ON M-PLANE SAPPHIRE VIA MOCVD

ABSTRACT

In the past few years, semi-polar (11-22) GaN has attracted much intention in the field of optoelectronics including light-emitting diodes (LEDs), laser diodes (LDs) and photodetectors. Commercially, GaN-based optoelectronic devices are grown along c-plane direction. However, c-oriented GaN-based optoelectronics suffer from piezoelectric polarization, which hinders the device performances. Conversely, semi-polar (11-22) GaN exhibits almost zero piezoelectric polarization effect. Furthermore, as the GaN wurtzite lattice is inclined approximately 58° respective to c-plane, it provides more sites for doping incorporation such as indium, silicon, aluminium, etc. Therefore, the semi-polar (11-22) GaN is presumed to be one of a promising candidate for efficient device applications. However, semi-polar GaN suffers from numerous crystal defects during the epitaxial process leading to poor crystal quality as well as surface properties. For decades, various approaches have been implemented to achieve an enhanced morphological and crystal quality of semi-polar (11-22) GaN. These approaches include the epitaxial lateral overgrowth (ELOG), surface selective growth on patterned substrates (SSG), and overgrowth on nano-rod array templates. However, such approaches require additional complex *ex-situ* processes with the use of dielectric materials. In addition, studies have also shown enhanced crystal qualities upon the utilization of *in-situ* techniques such as AlN/GaN multilayer and SiN interlayer. Nonetheless, such techniques require additional metal sources. In this study, enhanced surface morphological and crystal properties of semi-polar (11-22) gallium nitride (GaN) was successfully achieved via implementing an In-Situ Multiple Ammonia Treatment (I-SMAT) method. Utilization of an optimized flow of ammonia (2.3 SLM), surface striations of semi-polar (11-22) GaN was reduced yielding RMS roughness of

3.07 nm. Low scan sizes of the surface reveal an evolution of the atomic-sized terraces to a rather uniformly arranged distribution resulting in narrowing/shallowing of the interfacial valleys. X-ray rocking curve (XRC) analysis implies that I-SMAT would facilitate dislocation reduction through a selective-area etching process consequently enhancing the crystal quality. Conversely, excessive ammonia flux during the I-SMAT would degrade the structural and morphological properties of the semi-polar epilayer whereby the alternating thin GaN epilayer would undergo the selective-area etching to the extreme.

Keywords: gallium nitride, semi-polar, epitaxy, crystal, dislocation, ammonia

PERTUBUHAN LAPISAN EPITAXY SEMI-POLAR (11-22) GaN PADA NILAM BERSATAH-M MELALUI MOCVD

ABSTRAK

Beberapa tahun kebelakangan ini, separuh kutub (11-22) GaN telah menarik perhatian dalam bidang optoelektronik termasuk diod pemancar cahaya (LED), diod laser (LD) dan pengesan cahaya. Secara komersil, peranti optoelektronik berasaskan GaN ditumbuhkan pada arah satah-c. Walau bagaimanapun, optoelektronik berasaskan GaN mengalami polarisasi piezoelektrik yang mengurangkan prestasi peranti. Sebaliknya, separuh kutub (11-22) GaN mempunyai hampir sifar kesan polarisasi piezoelektrik. Selain itu, apabila kekisi wurtzite GaN dicondong kira-kira 58° dari satah-c, ia menyediakan lebih banyak tapak untuk penggabungan doping seperti indium, silikon, aluminium dan sebagainya. Oleh itu, separuh kutub (11-22) GaN dianggap salah satu calon yang menjanjikan untuk peranti aplikasi tinggi. Walau bagaimanapun, GaN separuh kutub mengalami banyak kerosakan kristal semasa proses epitaxy yang menjejaskan kualiti kristal serta sifat permukaannya. Selama beberapa dekad, pelbagai pendekatan telah dilaksanakan untuk meningkatkan mutu morfologi dan kristal separuh kutub (11-22) GaN. Pendekatan ini termasuk pertumbuhan besar berhaluan epitaxy (ELOG), pertumbuhan selektif permukaan pada substrat bercorak (SSG), dan pertumbuhan besar pada templat tiang-nano bersusun. Walau bagaimanapun, pendekatan sedemikian memerlukan proses tambahan ex-situ yang kompleks dengan penggunaan bahan dielektrik. Di samping itu, kajian juga menunjukkan kualiti kristal yang dipertingkatkan melalui menggunakan teknik in-situ seperti lapisan bertingkat AlN / GaN dan lapisan bertingkat SiN. Walau bagaimanapun, teknik tersebut memerlukan sumber logam tambahan. Dalam kajian ini, sifat morfologi dan kristal permukaan separuh kutub (11-22) GaN berjaya dipertingkatkan melalui kaedah Rawatan Amonia Berkali In-Situ (I-SMAT). Dengan penggunaan aliran ammonia (2.3 SLM) yang dioptimumkan, bentuk permukaan separuh kutub (11-22) GaN berkurang kekasarannya sebanyak 3.07 nm. Saiz imbasan rendah pada permukaan menunjukkan evolusi teres bersaiz atom kepada pertaburan yang agak seragam menyempitkan ruang / mencetekkan kedalaman permukaan lembah. Analisis keluk ayunan X-ray (XRC) menunjukkan bahawa I-SMAT akan memudahkan pengurangan dislokasi melalui proses penghakisan kawasan berselektif dan seterusnya meningkatkan kualiti kristal. Sebaliknya, aliran ammonia yang berlebihan semasa I-SMAT akan merendahkan sifat-sifat struktur dan morfologi lapisan epitaxy GaN separuh kutub di mana lapisan nipis epitaxy GaN yang berselang-seli akan mengalami penghakisan kawasan berselektif yang berlebihan.

Kata Kunci: gallium nitrida, separuh kutub, epitaxy, kristal, dislokasi, amonia

ACKNOWLEDGEMENTS

First and foremost, I would like to say "Alhamdulillah" means all the praises and thanks to Allah, the God all Mighty for as given me the strength and endurance completing this work.

I would like to express my deep and sincere gratitude to my supervisor Dr. Azzuliani Binti Supangat for giving me the opportunity to do research and providing invaluable guidance throughout this research. I have learned a lot of things from her and inspired me to build a research institute base on her vision. She is my best teacher and my idol.

I am extremely grateful to both of my beloved parents, Anuar Bin Adam and Khamisah Binti Muhamad for their love, prayers, caring and sacrifices for educating and preparing me for my future. Also, I would love to express my thanks to my siblings for their genuine support and prayers.

Special thanks to my friends, Abdullah Haaziq and Dr. Omar Ayad Fadhil for their constant support and guidance throughout my master's degree. They have taught me everything they know and help me when I faced any problems.

I am extending my thanks and appreciations to LDMRC Lab members, Hilmi, Zulhakim, Ooi Chong Seng, Gary, Nazry, Rakif, Aliff, Anas, Adreen, Adilah Roslan, Syaza Nafisah, Anis, Azmina, Ismaliza, Diyana, Najiha, Najwa, and Liyana, Dr. Arif Sarjidan, and Dr. Azrina for their help and encouragement.

Finally, I would like to acknowledge the University of Malaya Research Grant (RP039B-18AFR) and Fundamental Research Grant Scheme (FP078-2018A) for project funding.

TABLE OF CONTENTS

LIST OF FIGURES

LIST OF TABLES

LIST OF SYMBOLS AND ABBREVIATIONS

φ : Azimuthal angle

θ : Diffraction angle

ω : Incident angle

χ : Tilt angle

λ : Wavelength

AlN : Aluminum nitride

NH_3 : Ammonia

AFM : Atomic force microscopy

BSFs : Basal stacking Faults

Ga : Gallium

GaN : Gallium nitride

HR-XRD : High-resolution x-ray diffraction

I-SMAT : In-situ multiple ammonia treatment

LED : Light Emitting Diode

LT : Low temperature

Mg : Magnesium

MOCVD : Metal organic chemical vapor deposition

MO : Metal-organic

CH_4 : Methane

N_2 : Nitrogen

PDs : Partial dislocations

PSFs : Prismatic Stacking Faults

QCSE : Quantum Clark Stark Effect

RMS : Root mean square

SF	:	Stacking Fault
SLM	:	Standard liter per minute
TDs	:	Threading dislocations
TMG	:	Trimethylgallium
UV	:	Ultraviolet
Uid	:	Unintentional doped
XRC	:	X-ray rocking curve

CHAPTER 1: INTRODUCTION

1.1 Introduction

In 1969, Maruska and Tietjen discovered wurtzite structured GaN exhibit direct bandgap approximately 3.14 eV room temperature realizing potential used of GaN for optoelectronic (Maruska & Tietjen, 1969). However, GaN crystal can only be attained from the epitaxy process is suffer from high defect density. A crystal defect in GaN will act as a non-radiative recombination center and perturbed the bandgap to be indirect bandgap. Until 1985, Hiroshi Amano and his team have successfully attained high crystal quality GaN epitaxial layer growth on sapphire substrate by introducing a low temperature (LT) aluminum nitride (AlN) buffer layer (H. Amano, Sawaki, Akasaki, & Toyoda, 1986). Then, Shuji Nakamura and his team successfully invented the first efficient blue light GaN-based LED with LT- GaN buffer layer in 1994 (Nakamura, Mukai, & Senoh, 1994). The invention of solid-state light source GaN is proven to be 10 times more efficient than the tungsten filament light bulb. Moreover, GaN-based LED has a longer lifetime as compared to the tungsten filament light bulb. It is reported that the invention of GaN-based LED lead to the reduction of global energy consumption by 50%. However, people discovered GaN lattice suffers from an internal polarization effect that limits the performance of GaN-based LED (Takeuchi, Amano, & Akasaki, 2000).

Typical GaN-based LED is fabricated on polar c-plane orientation. The c-plane orientation exhibit spontaneous and piezoelectric effect polarization with obstruct the quantum level energy in the GaN including the bandgap energy (Takeuchi et al., 2000). The presence of intrinsic polarization generates internal electric field causing perturbation electron and hole wavefunction (Chen et al., 2017; Takeuchi et al., 2000). Thus, the disturbance of electron-hole wavefunction obstruct the electron and hole recombination and shifted the direct to indirect bandgap. Another issue faced by c-plane

GaN is Quantum Clark Stark Effect (QCSE) (Chen et al., 2017; Takeuchi et al., 2000). To fabricate long-wavelength visible light LEDs such as green and red light, a high indium ratio is required in InGaN lattice to reduce bandgap energy (Funato et al., 2006; Lin et al., 2000). However, due to large lattice mismatch between In GaN and InN in the InGaN structure, such structures suffer from large internal strain causing huge internal polarization field namely piezoelectric (strain-induced) polarization (Funato et al., 2006; Takeuchi et al., 2000).

However, all these issues can be solved by the growth of semi- and non-polar oriented GaN (Sasaki & Zembutsu, 1987; Takeuchi et al., 2000). In non-polar GaN, the GaN plane is perpendicular to the c-plane such as (10-10) and (11-20) plane (Konar et al., 2012; Romanov et al., 2011). As a result, bulk non-polar GaN exhibit zero polarization effect solving all fundamental issues discussed above. However, it is reported that non-polar oriented GaN surfaces shows low indium incorporation due to its stable and unreactive surface (Yamada et al., 2008). An alternative way to solve this issue is by growing semi-polar oriented GaN. Semi-polar GaN is an inclined plane between polar and non-polar GaN (Konar et al., 2012; Romanov et al., 2011). By this, semi-polar surface exhibits high indium incorporation as compared to polar and non-polar GaN. This is because inclined GaN surface providing many dangling bonds and sites for indium vacancies (Y. Zhao et al., 2012). Also, bulk semi-polar GaN induced a relatively low piezoelectric polarization effect compared to polar GaN. For example, semi-polar (11-22) GaN exhibits almost zero polarization effect. Therefore, semi-polar (11-22) GaN is considered a promising GaN plane for highly efficient long-wavelength LED.

Nevertheless, to date, semi-polar (11-22) GaN greatly suffers from threading dislocations (TDs) and stacking faults (SFs) (Omar, Shuhaimi, Makinudin, Khudus, & Supangat, 2018; Song, Oh, & Lee, 2013). Due to un-natural growth and large lattice mismatch between GaN and substrates, numerous crystal defect is generated at the interface. As consequences, inclined GaN crystal defects can extend from the epilayer to the surface. High crystal defect propagates to the surface will create a valley or pits causing surface degradation (Ahmad Makinudin et al., 2019; Song et al., 2013). Several methods have been introduced in attempt to reduce this defect. In this work, we will introduce in-situ multiple ammonia treatment (I-SMAT) for crystal and morphological enhancement of semi-polar (11-22) GaN epilayer via metal organic vapor deposition (MOCVD).

1.2 Aim and Research Objectives

The growth of semi-polar (11-22) GaN epitaxial on m-plane (10-10) substrate sapphire via MOCVD suffers from high defect density. Unlike polar orientated GaN, both dislocations and basal stacking faults (BSFs) in the semi-polar (11-22) GaN lattice propagate to the surface resulting in rough surface roughness. For decades, various approaches have been implemented to overcome these issues. These approaches include the epitaxial lateral overgrowth (ELOG) (Ni et al., 2007), selective growth on patterned substrates (SSG) (N. Okada, A. Kurisu, K. Murakami, & K. Tadatomo, 2009a), and overgrowth on nano-rod array templates (Zhang et al., 2016). However, such approaches require additional complex *ex-situ* processes with the use of dielectric materials. In addition, studies have also shown enhanced crystal qualities upon utilization of *in-situ* techniques such as AlN/GaN multilayer (Omar, Shuhaimi, et al., 2018) and SiN interlayer (Jeong et al., 2013). Nonetheless, such techniques require additional metal sources. Hence, this work aims to achieve high crystal quality and smooth surface roughness of semi-polar (11-22) GaN epitaxial through simple epitaxy technique. In this study, semi-polar (11-22) GaN epilayer will be grown with the assist of an in-situ multiple ammonia treatment (I-SMAT) technique: whereby a selective-area etching process occurs for multiple periods to obtain an enhanced structural and morphological properties of semi-polar (11-22) GaN epilayer.

The objectives of this work are:

1) To enhance the crystal quality and morphology of the semi-polar (11-22) GaN epitaxial layer via in-situ multiple ammonia treatment (I-SMAT).

2) To optimize the number of pairs and ammonia flux implemented in I-SMAT toward an enhancement of the semi-polar (11-22) GaN epitaxial layer.

3) To investigate the impact of I-SMAT on crystal defects in semi-polar (11-22) GaN.

CHAPTER 2: LITERATURE REVIEW

2.1 Gallium Nitride

Gallium Nitride is a direct wide bandgap III-V semiconductor that is commonly used in light-emitting diode (LED) (Maruska & Tietjen, 1969). Its stable compound properties allow it to withstand high temperature and low chemical reactivity with other materials. Moreover, GaN crystal exhibit 10 times greater power density than silicon (H Amano et al., 2018). Therefore, GaN is considered a future semiconductor material replacing other types of semiconductors. However, the growth of the high crystal quality of GaN epitaxial layer is challenging. It required an isolated reactor with precise controllable MO source flow and thermodynamic parameters (Koukitu, Takahashi, & Seki, 1997). Temperature above 1000°C is one of the importance thermodynamic parameters to grow high crystal quality GaN crystal in film form (Koukitu et al., 1997). Moreover, high substrate quality is needed for the growth of GaN. Impurity such as carbon and oxygen causing defect formation in GaN (Reitmeier, Park, Mecouch, & Davis, 2004). Defect in the GaN crystal will reduce the lifetime and act as non-radiative recombination center (Rieger et al., 1996; Sugahara et al., 1998). Therefore, the high crystal quality of GaN epitaxial layer is extremely hard to attain until 1986 when Hiroshi Amano successfully attained high crystal quality of GaN epitaxial layer by introducing LT-AlN buffer layer on the sapphire substrate as illustrated in Figure 2.1(a) (H. Amano et al., 1986). Then, Shuji Nakamura improvised his technique and invented the first efficient blue light LED using LT-GaN buffer layer as demonstrated in Figure 2.1(b) (Nakamura et al., 1994) .

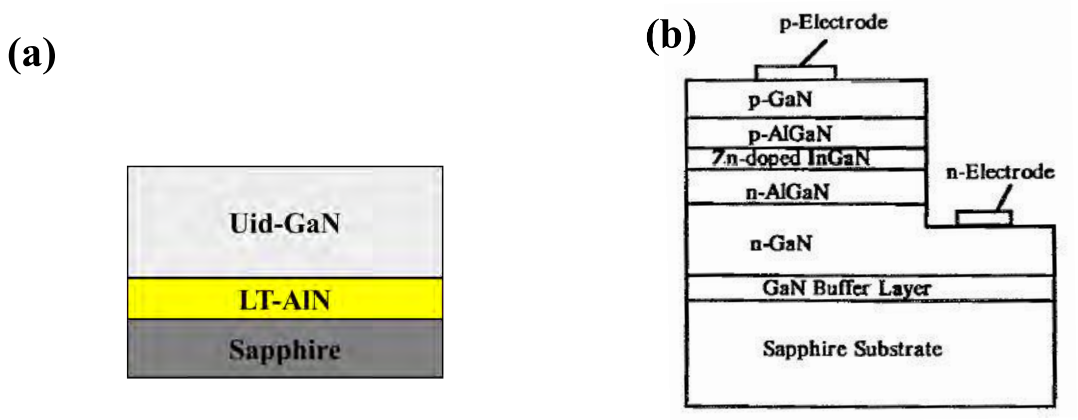

Figure 2.1: (a) Structure introduce by Amano (H. Amano et al., 1986) and (b) blue LED structure by Shuji Nakamura (Nakamura et al., 1994).

Since then, a whole range of light spectrum LED has been invented from UV to red wavelength by alloying with InN and AlN compound. High efficiency of GaN-based laser diode, solar cell, photodetector, and high electron mobility transistor also has been invented. The invention of the GaN-based LED lead to the reduction of global power consumption by 50%. However, the performance of LED devices has been limited by the internal polarization effect induced within Ga-N wurtzite lattice (Takeuchi et al., 2000). Most of the GaN-based devices is c-oriented plane whereby the Ga atoms and N atoms are arranged alternatingly along the surface normal as illustrated in Figure 2.2(a). Since Ga is positively charged and N is negatively charged, an alternating arrangement of both atoms will induce internal electric fields which are known as spontaneous polarization effect (Takeuchi et al., 2000). As stress or strain is introduced to the lattice, the hexagonal arrangement of Ga-N will be shortening and elongated along c-direction inducing net polarity as demonstrated in Figure 2.2(b). This net polarity will be induced an internal electric field. The higher the stress/strain, the greater the electric field is generated. Such an electric field is known as the piezoelectric effect. The existence of both spontaneous and piezoelectric effect will perturb the electrons and hole wavefunction making electron-hole recombination is harder to occur (Sugahara et al., 1998; Takeuchi et al., 2000).

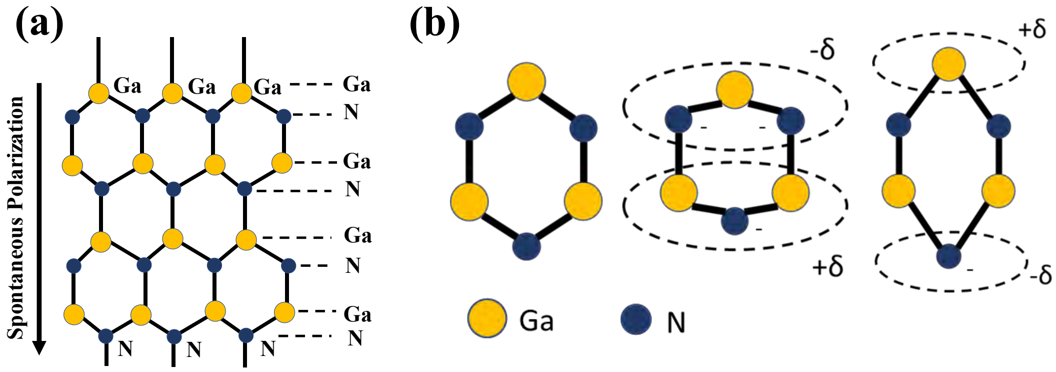

Figure 2.2: (a) The c-plane GaN lattice arrangement. (b) The piezoelectric effect induced in c-plane GaN.

As for device application, a higher current injection will assist greater perturbation of bandgap energy resulting lower density of electron-hole radiative recombination. In addition, the fabrication of long-wavelength LEDs such as red and green required a high ratio of Indium in InGaN composition to reduce the energy bandgap (Funato et al., 2006; Lin et al., 2000). In conventional c-plane GaN-based, the strain-induced piezoelectric fields are generated across the InGaN/GaN quantum well structures due to the lattice mismatch between the InGaN/GaN interface. Such polarization field will obstruct the electron and hole wavefunction at quantum well resulting less radiative recombination. This effect is known as Quantum Confined Stack Effect (QCSE) (Chen et al., 2017; Takeuchi et al., 2000). Therefore, semi-polar and non-polar oriented GaN is introduced to overcome this fundamental issue.

2.2 Non-polar and Semi-polar

The non-polar and semi-polar GaN has become a topic of interest in the V-III semiconductor field. This is because non-polar and semi-polar GaN exhibits none and low piezoelectric polarization effect, respectively. Generally, in non-polar GaN, the GaN plane is oriented perpendicular to polar c-plane direction such as (10-10) and (11-20) GaN plane which is called as m-plane and a-plane, respectively as depicted in Figure 2.3(a) and (b) (Konar et al., 2012; Romanov et al., 2011). With this orientation, the Ga and N atoms are bonded side by side with no alternating sequence along the surface direction as depicted in Figure 2.3(a). Therefore, non-polar GaN exhibit zero spontaneous polarization effect. Moreover, non-polar GaN owing zero piezoelectric effect due to neutral net dipole moment either lattice is under stress or strained condition as demonstrated in Figure 2.3(d). Consequently, non-polar GaN is promising candidates for the fabrication of high-efficiency GaN-based devices.

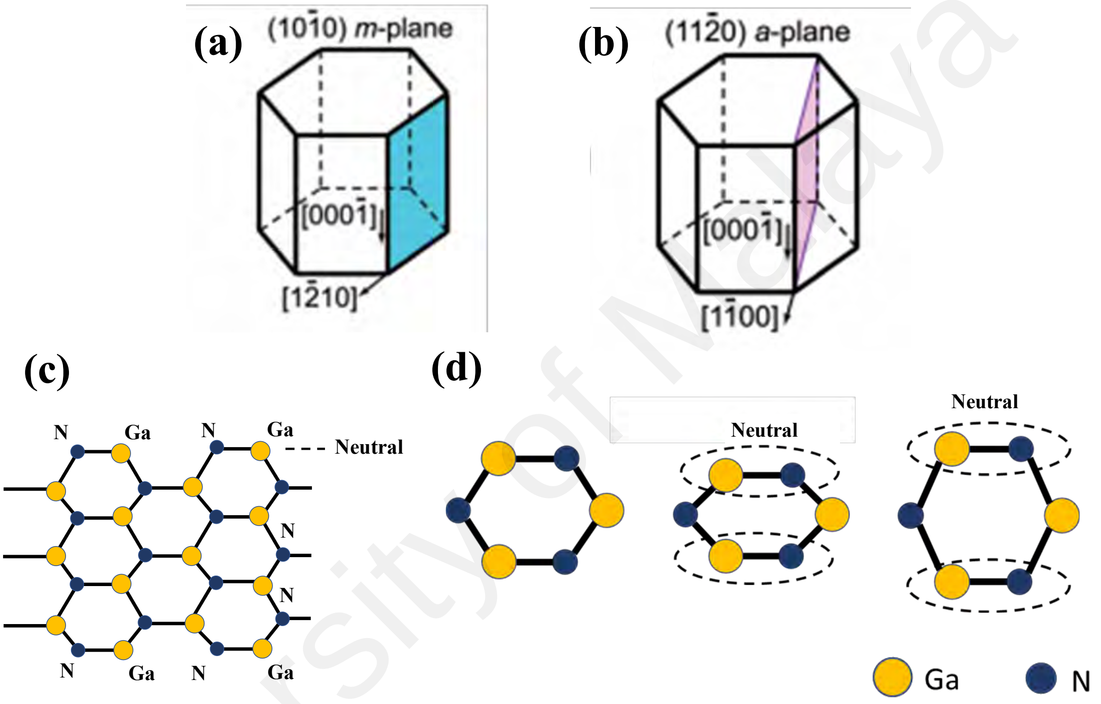

Figure 2.3: Non-polar plane of (a) (10-10) and (b) (10-20) plane (Romanov et al., 2011). (c) The Ga-N atom arrangement in non-polar GaN. (d) Piezoelectric effect on non-polar GaN.

On the other hand, the semi-polar plane is where the GaN crystal plane is oriented between the polar and non-polar plane. For example, (11-22) and (20-21) plane is inclined approximately ~58^{o} and ~75^{o}, respectively, to c-plane. As demonstrated in Figure 2.4(a), the lattice arrangement of inclined GaN resulting in closer alternating sequence between Ga and N atoms inducing lower spontaneous polarization effect as compared to polar GaN. Moreover, as demonstrated in Figure 2.4(b), the tilted lattice structure of semi-polar GaN generates a low piezoelectric polarization effect. Figure

2.4(c) shows the magnitude of the induced internal polarization field with the degree of inclination angle with respect to c-plane.

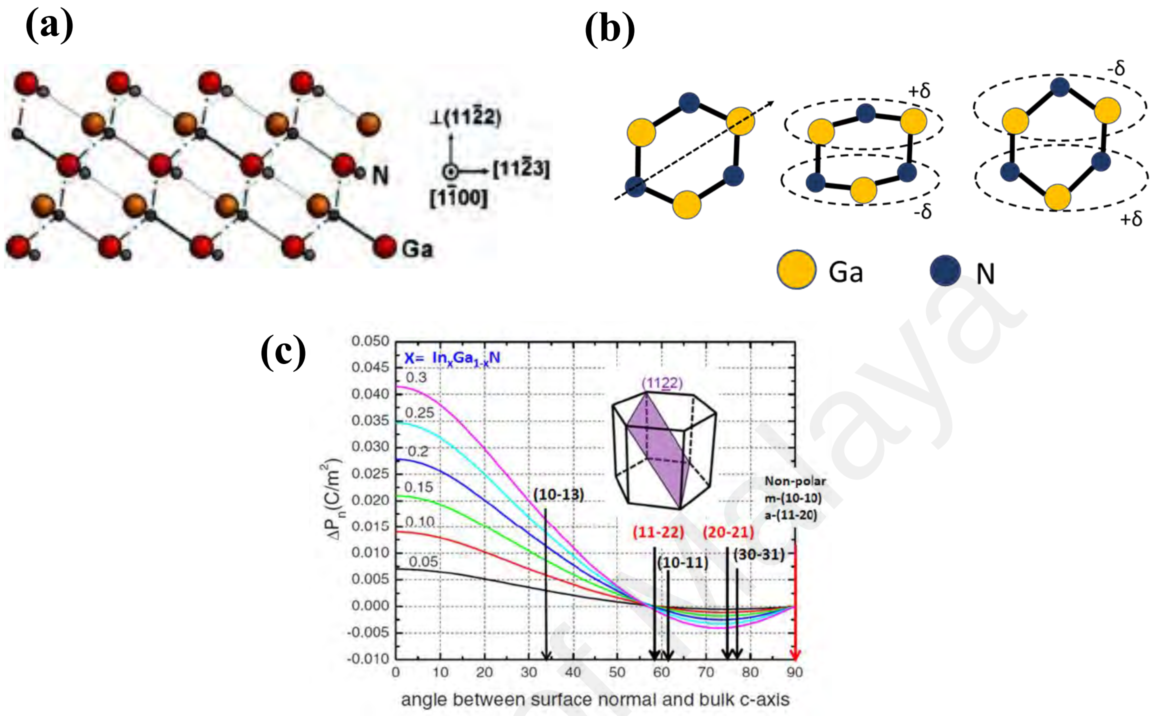

Figure 2.4: (a) The lattice structure in semi-polar (11-22) GaN (Das et al., 2010). (b) Piezoelectric polarization effect in semi-polar GaN. (c) Polarization effect of inclined plane from 0° to 90° (Wang, 2016).

In terms of polarization effect, non-polar GaN is seen as a better candidate for high-efficiency device application as compare to polar and semi-polar GaN. However, doping incorporation is a vital aspect that needs to be considered in device function. For example, fabrication of long visible wavelengths such as red and green light required high indium ration in the InGaN active layer to reduce the bandgap energy. Literature has reported that non-polar GaN exhibits low doping incorporation due to strong and stable Ga-N bond property of non-polar surface (Yamada et al., 2008). In contrast, semi-polar GaN is reported has high doping incorporation compare to polar and non-polar GaN (Y. Zhao et al., 2012). As polar GaN surface is tilted to a certain degree, the surface will be provided more dangling bonds and vacancies for any doping material such as indium, silicon, and magnesium (Y. Zhao et al., 2012). In semi-polar (11-22) GaN, first-principle calculation shows almost zero polarization effect. Therefore, some view semi-polar (11-22) GaN is an alternative way of fabricating highly efficient device applications. In this study, we will focus on semi-polar (11-22) GaN due to its high potential.

2.3 Defects in Gallium Nitride

A crystal structure is defined as the structure of atoms that are orderly arranged between each other. GaN with wurtzite structure is used as the base material in optoelectronic and power devices. However, crystal defect exists in the crystal will cause perturbation of electronic band from direct to indirect bandgap. In addition, crystal defects can act as non-radiative recombination centers and reduce device operation lifetime (Hangleiter et al., 2005; Rosner, Carr, Ludowise, Girolami, & Erikson, 1997). In this section, the type of crystal defects exits in the GaN wurtzite structure will be discussed in detail.

2.4 Threading Dislocation

Crystal dislocation occurs when there is an atomic displacement in part of a crystal lattice structure. In wurtzite structure, edge and screw dislocation are a general type of dislocation that occurs in the lattice and both are generated parallel to c-plane direction growth. Edge dislocation is a defect formed when an extra half-plane of atoms is inserted into one plane of the crystal lattice, distorting nearby planes of atoms (Yam, Low, Oh, Hassan, & Techniques, 2011). Meanwhile, screw dislocation can be conceived as atoms are displaced from the lattice causing new lattice to be tilted (Yam et al., 2011). The motion of both dislocations is the results of shear stress. Both dislocations are illustrated in Figure 2.5.

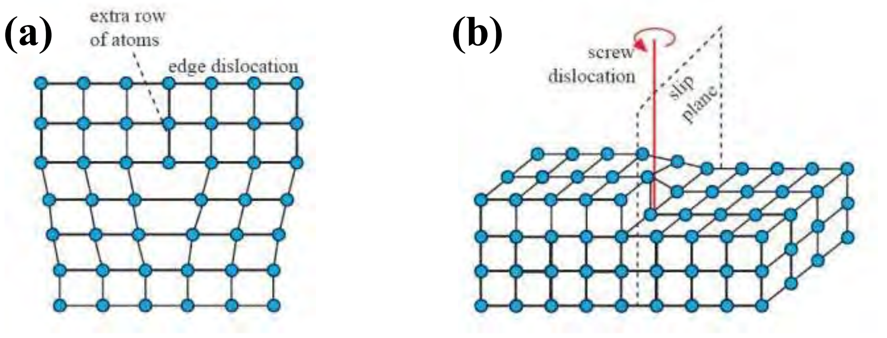

Figure 2.5: Schematic diagram of (a) edge and (b) screw dislocation (McNamara, 2009).

Both of dislocations are commonly combined and known as mixed dislocations. These dislocations are then defined as threading dislocations (TDs) as they propagate through the epitaxial layer. TDs can act as a nonradiative recombination center, carrier scattering effect and diffusion of dopant and impurities which can reduce the device efficiency and lower lifetime (Hangleiter et al., 2005; Rosner et al., 1997). In addition, TDs can form a pit as it successfully propagates to the surface degrading the morphology structure (Ahmad Makinudin et al., 2019; G. Zhao et al., 2016). The pit generated TD on the GaN surface will attract the oxygen to vacate and oxidize since pit are defect sites of GaN that are low energy bonded (Reitmeier et al., 2004).

2.5 Stacking Faults

Stacking faults (SFs) is a planar defect that alters the periodic sequence of the layers (Zakharov et al., 2005). In semi-polar GaN, the most dominant type of stacking fault formed BSFs in which occurs in a basal (0001) plane (Dasilva et al., 2010; Ni et al., 2007). Based on the literature, there are three types of BSFs that exist in the wurtzite structure: intrinsic(*I*) BSFs type I_1, intrinsic BSFs type I_2 and extrinsic(*E*) BSFs (Dasilva et al., 2010; Zakharov et al., 2005). The intrinsic I_1 type BSFs altered the perfect plane stacking sequence of …ABABABAB… to ABAB**AB**CBCBC… The intrinsic I_2 type BSFs altered the perfect plane stacking sequence of …ABABABAB… to ABAB**ABCAC**ACA… The *E* type BSFs altered the perfect plane stacking sequence of

…ABABABAB… to …ABA**BC**ABAB… The resulting stacking sequence by all BSFs types are demonstrated in Figure 2.6 (a)–(c).

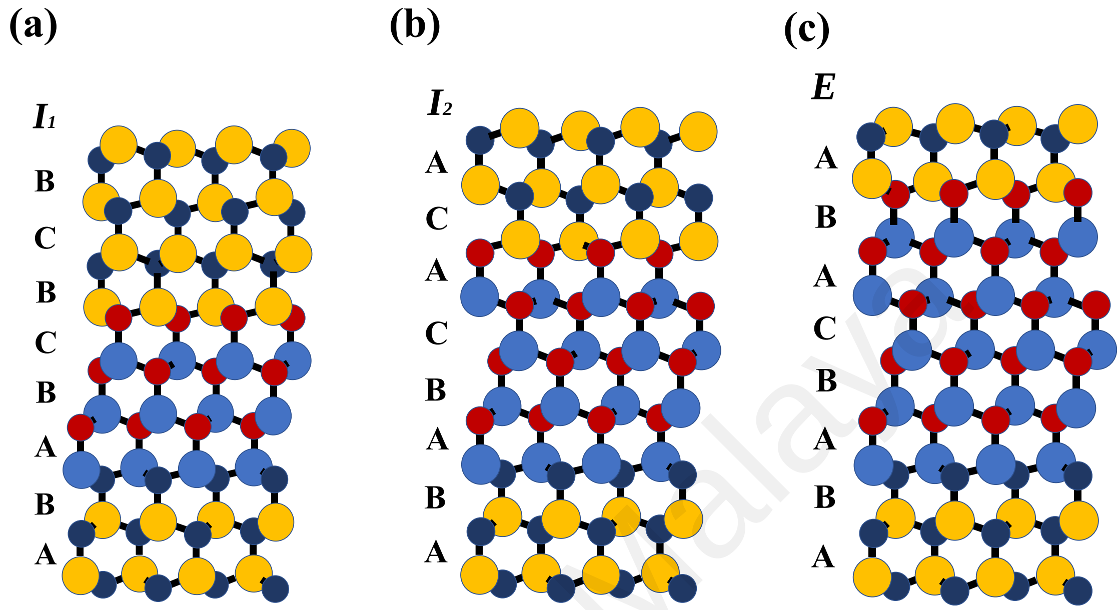

Figure 2.6: Atomic models of (a) I_1, (b) I_2, and (c) E type BSFs within wurtzite structure projected along the (11-20) plane.

As seen in Figure 2.6, BSFs type I_1 is formed either by removal or insertion of a basal plane with further 1/3 <1-100> slip of one part of a crystal respectively to other (Dasilva et al., 2010). Such fault is bounded by a sessile Frank-Shockley dislocation with Burgers vector b=1/6<20-23> (Dasilva et al., 2010). While BSFs type I_2 can occur by 1/3<1-100> of one part of crystal or by dissociation of perfect dislocation (b=1/3<11-20>) into two Shockley partial (b=1/3<1-100>) (Dasilva et al., 2010). Such faults are consequence of stress present during and after growth by the movement of glissile Shockley dislocation in the basal plane (Zakharov et al., 2005). As for BSFs type E, such fault is generated by precipitation of point defects on the basal plane with displacement vector of 1/2<0001> and surrounded by dislocation loop (Zakharov et al., 2005). This fault is bounded by frank partial dislocations (PDs). The formation energy of BSFs increase from type I_1, I_2 and E. This energy is increase with increment of the number of breaches in stacking sequence. From Figure 2.6, type I_1 BSFs are the most discerned defects owing to its lowest energy formation. Another common type of stacking fault founded in the wurtzite structure is prismatic stacking faults (PSFs). PSFs occur on prismatic {11-20} planes with fault vector of ½<10-11> (Dasilva et al., 2010; Zakharov et al., 2005). Report by Zakharov et al. 2005, one PSFs can be in connection with I_2 type BSFs (Zakharov et al., 2005). The summary of BSFs type with its bounded dislocation is tabulated in Table 2.1

Table 2.1: The type of BSFs with fault vector, stacking sequence and it bounded dislocation.

BSFs type	Fault vector	Stacking sequence	Bounded dislocation
I_1	1/6[20-23]	ABABCBCBC	Frank-Shockley dislocation
I_2	1/3[1-100]	ABABCACAC	Shockley partial dislocation
E	1/2[0001]	ABABCABAB	Frank partial dislocation

2.6 Techniques toward the enhancement of semi-polar (11-22) GaN crystal quality

Semi-polar (11-22) GaN epitaxial layer suffers from an abundance of stacking faults and dislocations. The various techniques have been introduced in an attempt to reduce these defects. In this subchapter, some of these techniques will be discussed in general due to its popularity and have been globally implemented.

2.6.1 Homoepitaxy

Homoepitaxy is an epitaxy process conducted on the substrate of the same material. For example, the growth of GaN epitaxial layer is conducted on a free-standing GaN substrate. Therefore, the lattice and thermal coefficient mismatch can be greatly reduced thus high crystal quality of semi-polar (11-22) GaN epitaxial layer can be attained.

Several reports have proven semi-polar (11-22) GaN epitaxial layer can be grown with low defect densities using semi-polar (11-22) GaN bulk substrate (Fujito, Kubo, &

Fujimura, 2009; Funato et al., 2006; Raring et al., 2011). However, this method can only be done on a small scale due to the small size of bulk GaN substrate. This is because bulk GaN substrate can be obtained by accurately cleaving a c-orientated (0001) thick GaN substrate with a few millimeters of thickness along with a non- and semi-polar direction. Therefore, the bulk GaN substrate is produced in small size and very expensive.

2.6.2 Heteroepitaxy

Heteroepitaxy is the growth of epitaxial layer on foreign substrates such as GaN on Si substrates and GaN on substrates. The purpose of using foreign substrates is to reduce the cost of GaN epitaxy process. The sapphire and silicon substrates are relatively cheaper and come with a bigger size compare to the GaN substrate. Therefore, heteroepitaxy is considered an alternative approach to cost-effective epitaxy processes that are more acceptable by industry. It has been reported that semi-polar (11-22) GaN epitaxial layer has been successfully grown on m-plane sapphire substrates (Ahmad Makinudin et al., 2019; Dasilva et al., 2010; Omar, Bakar, et al., 2018; Omar, Shuhaimi, et al., 2018; Sun, Leung, Yerino, Zhang, & Han, 2009). However, the growth of semi-polar (11-22) GaN epitaxial layers on m-plane sapphire substrates is challenging. Numerous literatures have reported semi-polar (11-22) GaN epitaxial layer on m-plane sapphire suffers from high crystal defects densities of stacking faults and dislocations (Agrawal, Radhakrishnan, Dharmarasu, & Pramana, 2015; Sun et al., 2009; Xu et al., 2012). The high density of stacking faults and dislocations are generated by large lattice mismatch and thermal coefficient between GaN epilayer and sapphire/silicon substrates (Agrawal et al., 2015; Sun et al., 2009; Xu et al., 2012). As consequences, these crystal defects can propagate to the surface degrading the surface structure (Ahmad Makinudin et al., 2019). In addition, non-optimize growth conditions can lead to mixed-phase growth of semi-polar (11-22) and (10-13) GaN (Omar, Bakar, et al., 2018; Ploch et al., 2010). This, in turn, resulting in lower crystal quality and surface morphology due to the twinning effect of (10-13) GaN growth in two different directions (Omar, Bakar, et al., 2018; Ploch et al., 2010). Therefore, single-crystalline (11-22) GaN overgrown on m-plane sapphire is difficult to attain.

2.6.3 Epitaxial Lateral Overgrowth (ELOG)

It is impractical to use small and very expensive GaN substrate (homoepitaxy) for the growth of semi-polar (11-22) GaN. On the other hand, the growth of semi-polar (11-22) GaN on a planar m-plane sapphire substrate (heteroepitaxy) suffers high crystal defect density due to large lattice mismatch between GaN and sapphire interface. Therefore, Epitaxial Lateral Overgrowth (ELOG) technique was introduced for a more cost-effective and larger-scale approach.

Generally, ELOG techniques involve control of epitaxy mode by a patterning process. In this technique, the semi-polar (11-22) GaN epitaxial layer was grown on inclined or tilted (0001) surface to make the in-plane with ~58° to the surface normal. Therefore, the crystal quality of semi-polar (11-22) GaN is expected to be equal to the growth of c-plane GaN. Many literatures have reported a high crystal of semi-polar (11-22) GaN has been achieved by this method (Ni et al., 2007; Okada et al., 2009a).

Conventionally, semi-polar (11-22) GaN epitaxy by the ELOG process involves patterning by lithography and deposition of dielectric material, namely silicon dioxide (SiO_2) or silicon nitride (SiN_x). For instance, Ni et al employed the ELOG technique by depositing a thin SiO_2 layer on standard (11-22) GaN epitaxial layer that has been grown directly on m-plane sapphire (Ni et al., 2007). This standard (11-22) epitaxial layer was first obtained by a two-step growth method and exhibit highly broad x-ray rocking curve FWHM indicating a high crystal defect. Then, the 140 nm of SiO_2 layer was deposited on the surface of standard semi-polar (11-22) GaN by using plasma-enhanced chemical vapor deposition. A standard lithography technique was implemented to form a uniform 10 µm SiO_2 stripes with 4 µm windows along [1-210] a-plane direction as shown in Figure 2.7(a). After the patterning process, the sample was again undergoing an epitaxy process inside the MOCVD chamber. As a result, a c-plane GaN facet was formed with the inclination of 32^o to the substrate surface as shown in Figure 2.7(b). High crystal quality of semi-polar (11-22) GaN was achieved by a great reduction of dislocation and BSFs.

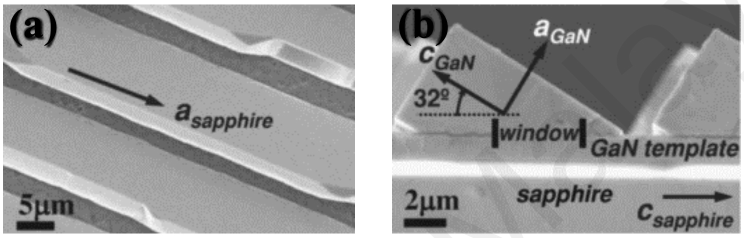

Figure 2.7: ELOG technique introduce by Ni et al. with its SEM images of (a) surface, and (b) cross-sectional (Ni et al., 2007).

Another popular technique in the growth of semi-polar (11-22) GaN film by using ELOG is introduced by Okada et al. (N. Okada, A. Kurisu, K. Murakami, & K. J. A. p. e. Tadatomo, 2009b). In this technique, the patterned r-plane sapphire substrate was used to grow semi-polar (11-22) GaN epitaxial layer as illustrated in Figure 2.8. The inclination angle of the r-plane and (11-22) plane from the c-plane is almost equal which is 57.6^o and 58.4^o, respectively. Thus, if GaN growth on c-plane surface sidewall of the r-plane sapphire substrate, a surface normal of the GaN will be (11-22) GaN facet producing semi-polar (11-22) GaN epitaxial layer. The growth of semi-polar (11-22) GaN epitaxial layer by this technique is reported to attain high crystal quality with no issue of unintentional growing semi-polar (10-11) that causing polycrystalline crystal. To pattern the r-plane sapphire substrate to form c-plane sidewall, a standard photolithography and dry etching techniques using inducing coupled plasma (ICP) or reactive ion etching (RIE).

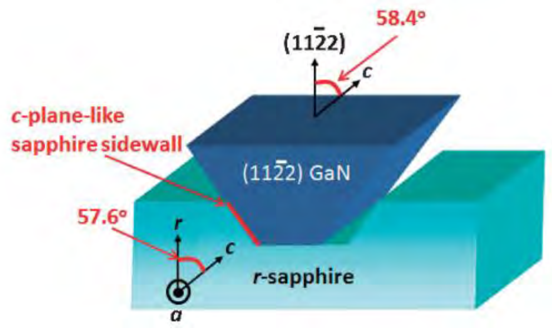

Figure 2.8: Growth of semi-polar (11-22) GaN epitaxial layer on patterned r-plane sapphire substrates (Okada et al., 2009).

Although this approach seems promising, it requires additional steps, additional instrument, time-consuming, complicated and sometimes required regrowth process (ex-situ). Moreover, since ELOG techniques is a selective growth epitaxy, it has an intrinsic non-uniformly issue in both crystal quality and surface morphology.

2.6.4 Ammonia Gas Treatment

Currently, the simplest technique used toward the enhancement of semi-polar (11-22) GaN epitaxial layer is ammonia gas treatment introduced by Song et. al. (2013). In their technique, the ammonia gas is applied on the surface of the underlying thin GaN layer at 1040°C for 10 minutes. As a result, the improvement of crystal quality semi-polar (11-22) GaN epitaxial layer was observed from a reduction of x-ray rocking curve FWHM value on [-1-123] and [1-100] diffraction plane. In addition, the surface morphology was enhanced by the decrease of RMS surface roughness to 62.8 nm measured by atomic force microscopy (AFM). They reported the enhancement of crystal quality by this approach was due to the GaN thermal etching process at the underlying thin GaN epitaxial layer by ammonia gas at high temperature. Based on the literature, a crystallographic plane of (11-22), {10-10} and {10-11} GaN facet can be exposed by a chemical wet etching process (Tamboli, Hirai, Nakamura, DenBaars, & Hu, 2009; Zhuang, Edgar, & Reports, 2005). Among these planes, (11-22) GaN has higher thermal instability. As ammonia treatment is implemented, the (0001) and {10-10} GaN plane were undergone desorption leaving (11-22) GaN plane dominating on the surface. The domination of (11-22) GaN plane on the surface provides smoother surface roughness and promotes a more stable condition of semi-polar (11-22) GaN epitaxy that leads to crystal and morphology enhancement. Nevertheless, the mechanism of surface and crystal enhancement of this work do not explain and discussed in detail due to a lack of x-ray diffraction and atomic force microscopy analysis. Figure 2.9 displayed the typical arrowhead-like feature on semi-polar (11-22) GaN surface as reduced as ammonia treatment was employed onto the underlying layer.

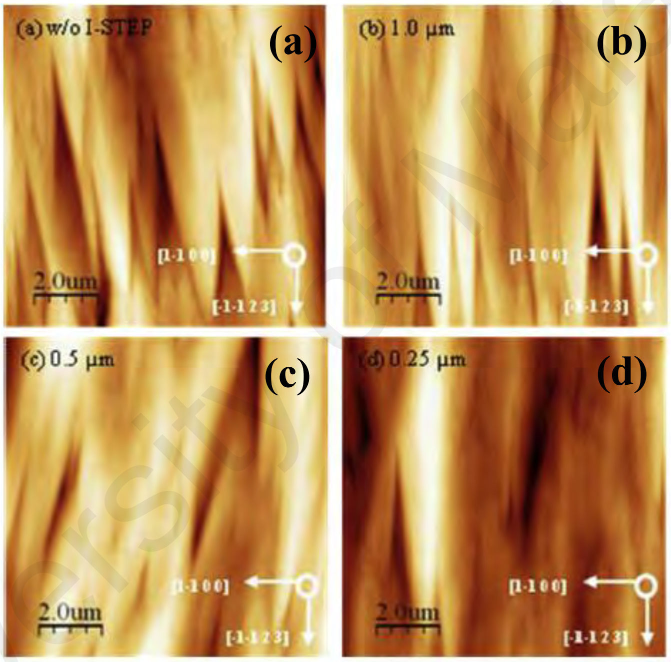

Figure 2.9: Atomic Force Microscopy (AFM) images showing surface enhancement by ammonia treatment (Song et al., 2013).

By comparing with other mentioned techniques, in term of device fabrication and application, ammonia treatment has the advantages such as facile, cheaper and faster technique to enhance crystal quality. These advantages give more flexibility for device structure modification. In LED and transistor, there are many types of device structure that have its own beneficial characteristic. Since there is no material other than GaN on underlying buffer GaN layer, electrode contact on the underlying layer can be implemented.

Inspired by this brilliant work, we believe this technique can be ameliorated and integrate to become more effective toward the enhancement of crystal quality and morphology of semi-polar (11-22) GaN epitaxy. In this study, we implemented a multiple thin GaN epitaxial layer treated with ammonia gas on the underlying layer called in-situ multiple ammonia treatment (I-SMAT). This technique promotes greater crystal and morphological enhancement of semi-polar (11-22) GaN epitaxy with a shorter time to implement ammonia flux. The detail of in-situ multiple ammonia treatment (I-SMAT) is explained in Chapter 3 and the outcomes of the work are further discussed in Chapter 4.

CHAPTER 3: EXPERIMENTAL AND CHARACTERIZATION METHODS

This chapter discusses the instruments and materials used throughout this work. The metal-organic chemical vapor deposition (MOCVD) general operating mechanism is discussed in detail. In addition, the chemical reaction occurs in the MOCVD reactor is described in terms of thermodynamic. Then, the experimental method prior to in-situ multiple ammonia treatment (I-SMAT) is discussed. Finally, the characterizations method utilized to study the effect of I-SMAT toward the enhancement of crystal quality and morphology of the semi-polar (11-22) Unintentionally doped (Uid) -GaN grown on m-plane sapphire substrate are properly explained.

3.1 Metal-Organic Chemical Vapor Deposition (MOCVD)

In this work, the gallium nitride epitaxy was carried out via metal-organic chemical vapor deposition (MOCVD). This technology can precisely control the gas laminar flow, temperature, and pressure in the reactor for the epitaxy process. Figure 3.1(a) and (b) shows the schematics of the MOCVD reactor design to inhibit turbulence in the gas flow resulting in precise control of film thickness. The metal-organic (MO) precursor was used is Trimethylgallium (TMG) react with ammonia gas to produce gallium nitride and methane as shown in Equation (3.1). The vapor pressure of metal-oxide and ammonia gas is low and needs to be carried by high vapor pressure gasses. For metal-oxide, the gas carriers are hydrogen and nitrogen while for ammonia is nitrogen. The flow rate of the metal-oxide and ammonia can be controlled by its gas carrier. During the epitaxial process, the substrate will be heated to the desired temperature. The temperature that can achieve by MOCVD, Taiyo Nippon Sanso Model SR-2000 used in this project is from room temperature to 1180^{o}C. The waste product of the reaction flows out through the exhaust. In this work, the Taiyo Nippon Sanso SR-2000

MOCVD was utilized to grow a semi-polar (11-22) GaN crystal. Figure 3.2 shows the photograph of Taiyo Nippon Sanso SR-2000 MOCVD.

$$(CH_3)_3Ga + NH_3 \rightarrow GaN + 3CH_4 \tag{3.1}$$

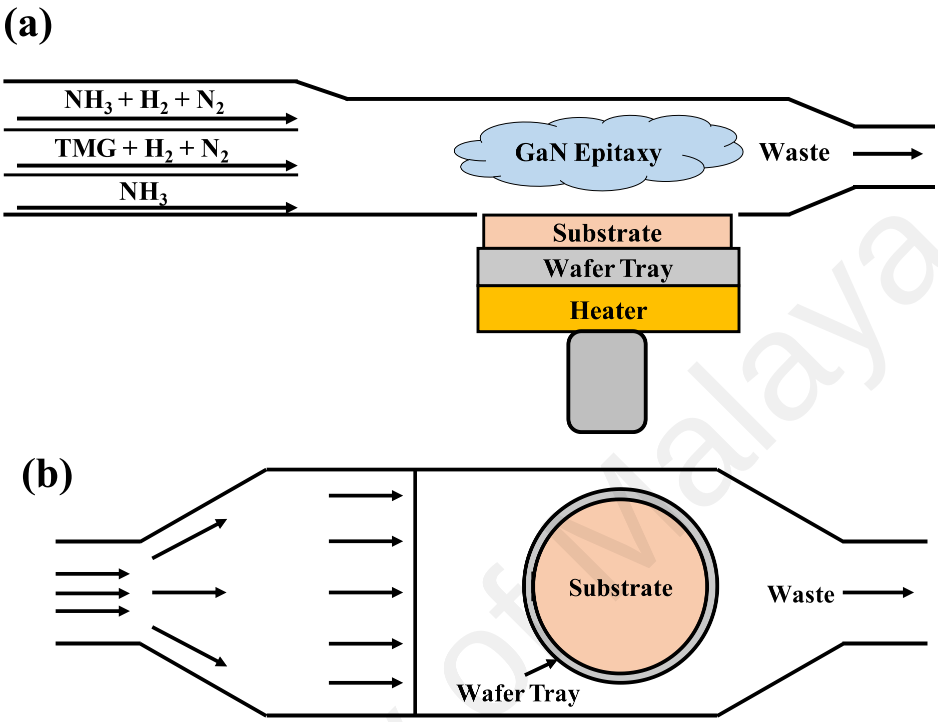

Figure 3.1: The schematic diagram of MOCVD reactor of (a) cross-section view and (b) plane view.

Figure 3.2: The Taiyo Nippon Sanso SR-2000 MOCVD.

3.2 Growth Methodology

The semi-polar (11-22) GaN epi-layers were grown on 2-inch m-plane (10-10) sapphire substrates via metal-organic chemical vapor deposition (MOCVD) (SR-2000, Taiyo Nippon Sanso, Japan). Trimethylgallium (TMG) and ammonia (NH_3) were used as the precursors for gallium (Ga) and nitrogen (N), respectively. A schematic illustration of the steps involved during the growth is depicted in Figure 3.3. Initially, (a) the substrate was cleaned via hydrogen ambient at 1125°C for 10 mins to remove any contaminated oxides layer on the surface of the substrate. Then, (b) nitridation was implemented on the sapphire substrates by applying 5 SLM of NH_3 flux at 1050°C. Next, (c) subsequent growth of 20 nm semi-polar (11-22) GaN prior to the I-SMAT process; NH_3 flowing alternately with 20 nm of GaN epilayer repeatedly for 20, 40 and 60 times, and followed by the growth of a 4.5µm thick Uid-GaN epilayer at 1050°C.Variation of the NH_3 flux was carried out at 0, 1 2.3 and 4 SLM and denoted as T0, T1, T2, and T3, respectively, to determine the impact of the I-SMAT technique. The implementation time of NH_3 flux was keep constant to 5.5 seconds and the V/II ratio utilized for GaN epitaxy is ~116.

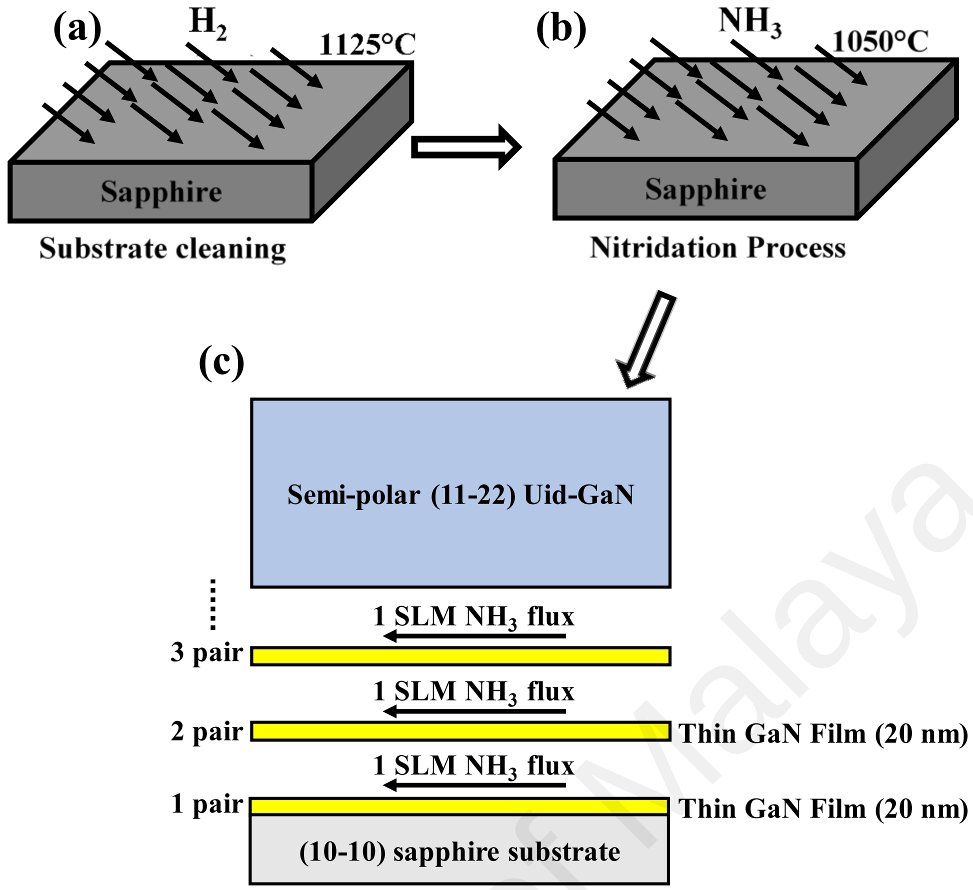

Figure 3.3: The schematic illustration of the growth of semi-polar (11-22) GaN with the I-SMAT technique.

3.3 Characterization Methods

The characterization of the semi-polar (11-22) GaN is this work has been carried out by atomic force microscopy (AFM), and high-resolution x-ray diffraction (HR-XRD). The AFM5000II atomic force microscopy (AFM) was conducted to analyse the surface morphology of the samples in detail. The anisotropic properties of the semi-polar (11-22) GaN was examined via the Rigaku high-resolution x-ray diffraction (HR-XRD) including 2θ-ω phase analysis (PA), On- and Off-axis x-ray rocking curve (XRC).

3.3.1 Atomic Force Microscopy

The sample surface morphology was further characterized by AFM measurement. Unlike FESEM, AFM is a very-high-resolution scanning probe microscopy that capable to provide 2D and 3D information on the surface within a micrometer to nanometer scale. Therefore, the surface morphology of the sample can be analyses in detail. In this work, the AFM 5000II instrument is used as shown in Figure 3.4 . During the measurement, the tapping mode is used whereby the tip is in contact with the surface and lifted off the surface to prevent dragging across the surface. As a result, high-resolution images and more accurate analysis can be obtained.

Figure 3.4: The image of AFM5000II instrument.

The schematic of the working principle of the AFM is demonstrated in Figure 3.5. Generally, AFM consists of a tip attached with cantilever, laser, and quadrant detector. During the measurement, depends on scan mode, the tip will or will not in contact with the sample surface. The atomic force between the tip and the sample surface leads to the deflection of the cantilever according to Hooke’s law. Concurrently, the laser beam is shouted on the backside of the cantilever and deflected to the quadrant detector. As the deflection of cantilever increases, the degree of the laser deflected increases. The quadrant detector measures the degree of the laser deflection and transfers the information to the software for the 3D imaging process. After scanning the whole sample surface, a 3D image can be obtained. Sample preparation such as sample cleaving and ozone cleaning is required before the AFM measurement.

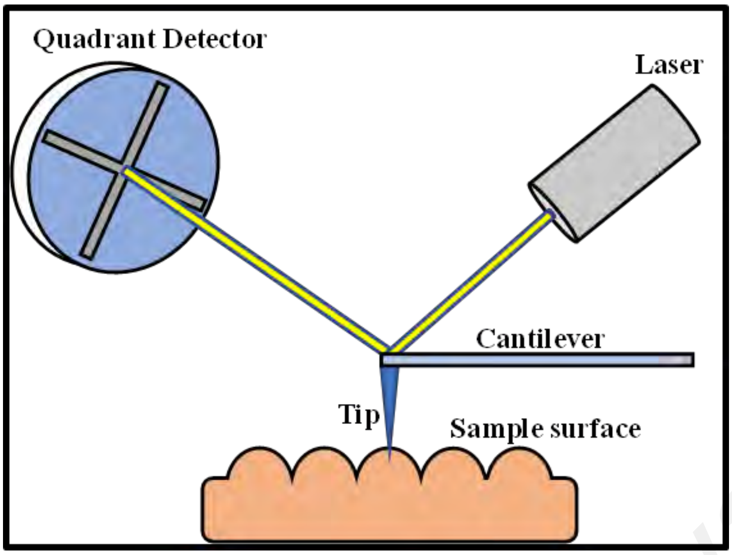

Figure 3.5: The schematic diagram of basic AFM working principle.

3.3.2 X-ray Diffractometer

The x-ray diffractometer instrument typically consists of the x-ray source, a sample stage (goniometer) and x-ray detector as illustrated in Figure 3.. In this system, the x-ray source generates x-ray radiation by a bombardment of high energy electron to the metal (Ge). Then, the x-ray radiation is emitted through incident optics onto the sample that has been placed on the sample stage. The diffracted x-ray radiations were detected and measured by the detector via receiving optics. The goniometer is used to aligning the sample with the detector.

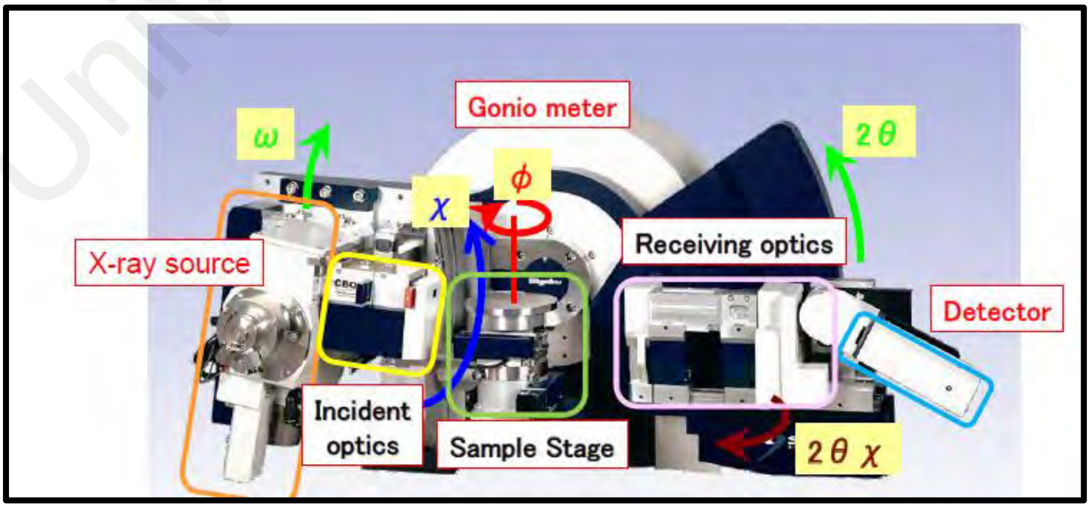

Figure 3.6: Rigaku HR-XRD system setup.

Prior to measurement, omega (ω) is defined as an incident beam angle respective to sample whilst 2 thetas (2θ) is an angle between the incident beam and x-ray detector. The x, y, and z position of the sample are precisely controlled by in-plane rotation angle, $\boldsymbol{\varphi}$ (rotate around z-axis) or Azimuthal angle, ω, and inclination angle, χ (rotate around the x-axis). Figure 3. illustrates the schematic diagram incident and the diffraction beam in the measurement and sample movement and rotation angle.

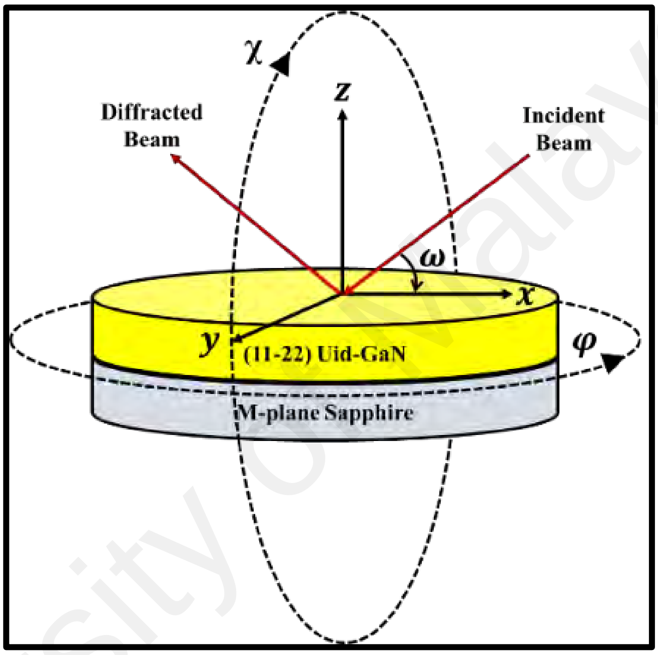

Figure 3.7: Schematic illustration of incident and diffraction beam with the sample movement and rotation angle.

3.3.3 High Resolution X-ray Diffraction (HR-XRD)

In this work, the crystallinity and anisotropic properties of the semi-polar (11-22) GaN epitaxial was characterized intensively by x-ray diffraction (XRD). In general, x-ray diffraction characterization is a non-destructive characterization because it emits x-ray radiation to the material and measures the intensity and angle of diffracted x-ray radiation governed by Bragg's law. Thus, the intensity and angle diffracted by material can be utilized to investigate the GaN crystal structure, orientation, crystallinity, and crystal defects.

Based on Bragg's law, the constructive interference occurs between the scattered x-ray as the path difference, $2d\ sin\vartheta$ is equivalent to an integer number of wavelengths, $n\lambda$ in which can be simply expressed by Equation (3.2)

$$2d\ sin\vartheta = n\lambda \tag{3.2}$$

Where d is the interplanar distance, ϑ is the incident angle with respect to the plane, λ is x-ray wavelength and n is the number of wavelengths.

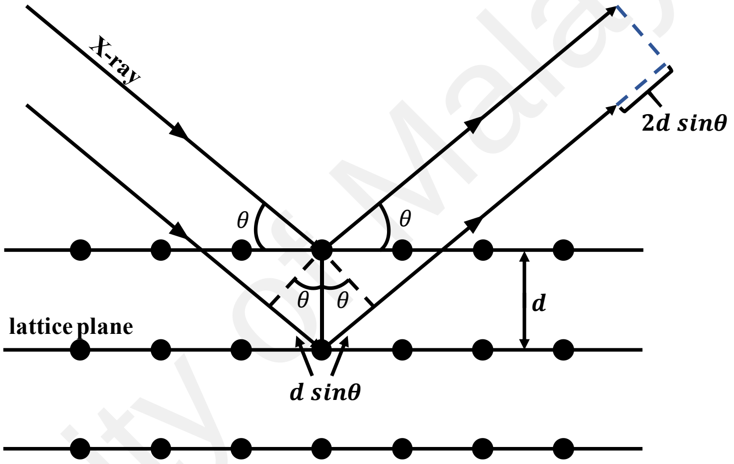

Figure 3.8: The diffraction of x-ray beam by atom in the crystalline structure.

Figure 3. demonstrated the relationship between the incident angle and diffraction angle based on Bragg's law and used in XRD measurement. As two identical x-ray radiation is radiated to the crystalline solid, it is diffracted by two different atoms. A lower beam transverses extra length of $2d\ sin\vartheta$ compared to the upper beam. A constructive interference occurs when this length is equal to an integer multiple of the wavelength of the radiation. This technique can be implemented to measure and determine the diffraction angle and interplanar spacing. In GaN, the crystal quality can be examined by the intensity of diffracted x-ray radiation at certain angle while interplanar spacing can be utilized to determine crystal orientation and crystal defects. In this study, the XRD characterization was carried out using the Rigaku HR-XRD.

3.3.4 X-ray Rocking Curve (ω-scan)

X-ray rocking curve (XRC) is a scanning mode measure the diffraction intensity along the reciprocal lattice vector to indicate the quality of crystalline lattice. As an example, the broadening of a specific peak angle is the result of a defect in the crystal. This method is performed as a function of ω with constant 2θ. In this work, the symmetric plane (On-axis) and asymmetric plane (Off-axis) XRC measurement were utilized to study the anisotropic properties and planar defects of the epitaxial layer, respectively.

In On-axis XRC measurement, the sample is rotated 360^o with φ around the surface normal while the detector is stationary. The incident beam projection at 0^o and 90^o was set [-1-123] and [1-100] crystal direction. This measurement was conducted to study the anisotropic properties of the sample and insensitive to crystal defect especially BSFs (Moram & Vickers, 2009; Sun et al., 2009). Thus, the Off-axis was employed to investigate the crystal defects in the lattice, namely partial and/or perfect dislocation and BSFs (Moram & Vickers, 2009; Sun et al., 2009). The Off-axis XRC diffraction planes conducted in this work are (10-11), (10-20), (10-10) and (0002). These diffraction planes were measured by aligning the φ and tilt (χ) with respect to the surface normal. Table 3.1 stated the values of ω, 2θ, and χ for each diffraction plane. The FWHM broaden factor for each Off-axis plane is listed in Table 3.2.

Table 3.1: The values of ω, 2θ, and χ for each diffraction plane.

Diffraction Plane	ω (^{o})	2θ (^{o})	χ (^{o})	Incident Beam Direction
(10-11)	18.43	36.95	26.18	**(101)**
(10-10)	16.24	32.48	42.48	**(100)**
(11-20)	28.97	57.95	31.61	**(110)**
(0002)	17.35	34.70	58.38	**(002)**

Table 3.2: Off-axis XRC planes with their broadening factor.

Off-Axis Plane	FWHM Broadening Factor
(10-11)	Perfect Dislocations
(11-20)	Prismatic Stacking Faults
(10-10)	Basal Stacking Faults (BSFs) Type I
(20-20)	Basal Stacking Faults (BSFs) Type II
(0001)	Partial and/or Perfect dislocations

3.3.5 Phase analysis (2θ/ω)

The phase analysis of 2θ/ω was utilized to investigate the crystal orientation of the epitaxial layer. Unlike On- and Off-axis XRC, phase analysis can determine the polycrystalline that exist in the crystal lattice. The 2θ/ω scan is done by rotating the sample stage by ω with a fixed detector at 2θ.

CHAPTER 4: RESULTS AND DISCUSSION

In this work, the effect of NH_3 and the number of pairs of I-SMAT employed towards the enhancement of crystal quality semi-polar (11-22) GaN epitaxial grown on m-plane (10-10) sapphire substrate is discussed. The anisotropic property and the crystal quality of the semi-polar (11-22) GaN epitaxial layer has been examined by using high-resolution x-ray diffraction (HR-XRD), inclusive of $2\theta/\omega$, On- and Off-axis x-ray rocking curve (XRC). In addition, the AFM characterization is utilized for each sample to investigate the impact of this treatment on the surface morphology. The NH_3 fluxes implemented in this work are 1, 2.3 and 4 SLM with various pairs of 20, 40 and 60. For simplicity, each sample is named with sample ID as displayed in Table 4.1 and the sample without treatment (bare Uid-GaN) is named as T0.

Table 4.1: The sample ID for each sample.

NH_3 Flux (SLM)	**Number of Pairs**		
	20	**40**	**60**
1 (Low)	T1 20	T1 40	T1 60
2.3 (Intermediate)	T2 20	T2 40	T2 60
4 (High)	T3 20	T3 40	T3 60

4.1 Impact of I-SMAT Implemented with 1 SLM of NH_3 flux

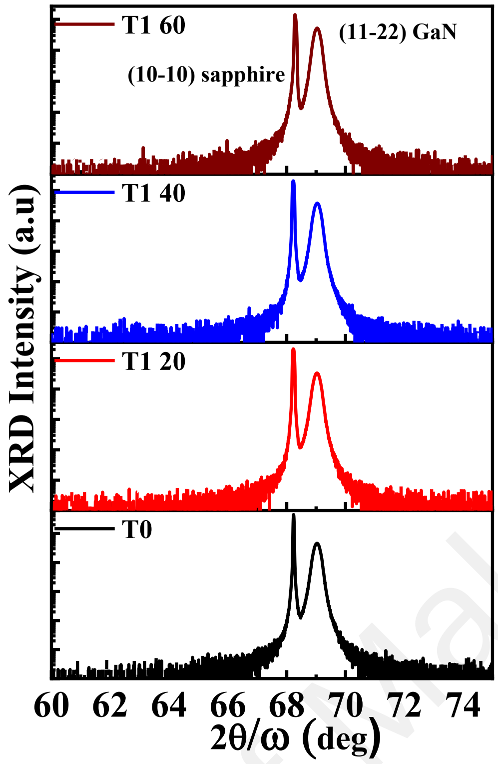

Figure 4.1: HR-XRD 2θ-ω scans of (11-22) Uid-GaN epitaxial layers grown on m-plane sapphire substrate for T0 and all T1 samples.

Figure 4.1 demonstrated the HR-XRD 2θ-ω scans of (11-22) Uid-GaN epitaxial layers grown on m-plane sapphire substrate for T0, T1 20, T1 40 and T1 60. Diffraction peaks were clearly observed at 68.2° and 69.0° attribute to m-plane (10-10) sapphire substrate and semi-polar (11-22) GaN, respectively. The HR-XRD 2θ-ω scans revealing all samples attained single crystalline (11-22) GaN on m-plane sapphire.

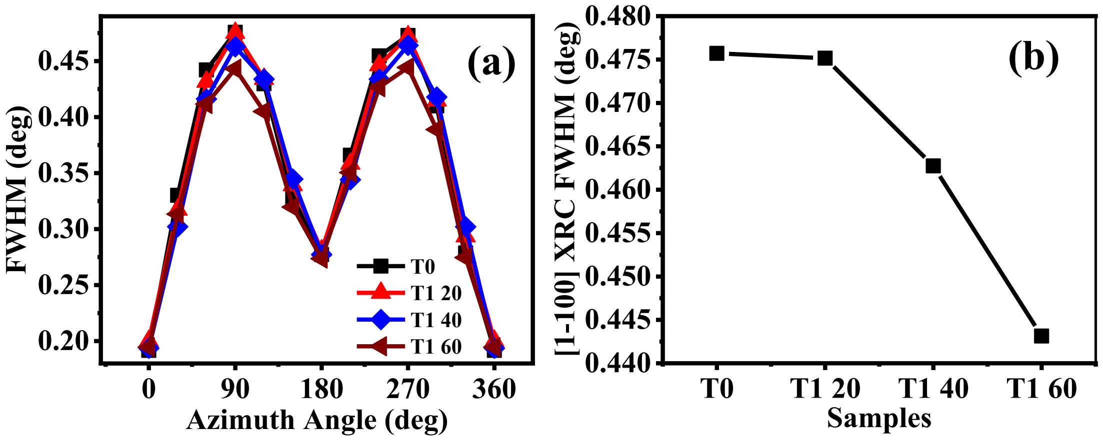

Figure 4.2: (a) On-axis XRCs FWHM of (11-22) GaN ω- scan as a function of azimuthal angle (Φ). (b) XRCs FWHM on [1-100] directions.

The anisotropic properties of the semi-polar (11-22) GaN epitaxial layer is analyzed via implementing the On-axis XRC measurement with various azimuthal angle Φ as demonstrated in Figure 4.2**.** The On-axis analysis was taken from 0° (equivalent to (-1-123) direction) to 360^{o} with an interval of 30° whereas, at 90°, the scanning direction is along (1-100). A strong anisotropic property was observed for T0 whereby the XRC FWHMs along [1-100] is broader than along [-1-123] owing to lattice mismatch between the semi-polar (11-22) GaN and the sapphire substrate. In Figure 4.2 (a) and (b), the XRC FWHM value progressively reduces as the pairs of I-SMAT employed increase. The T1 60 exhibits the least broadened FWHM along [1-100] indicating an enhancement of crystal quality. This suggest low implement of NH_3 flux required higher pairs for greater enhancement of semi-polar (11-22) GaN crystal quality. Studies have shown that the narrowing of the On-axis XRCs would be in direct correlation with the termination of dislocation densities (G. Zhao et al., 2016). Moreover, the value of FWHM XRCs on [1-100] direction can also be broaden by PSFs with a displacement vector of 1/2<10-11> (Frentrup, Ploch, Pristovsek, & Kneissl, 2011; Zakharov et al., 2005) which causes the FWHM at [1-100] to be broader than at [-1-123] direction for all samples.

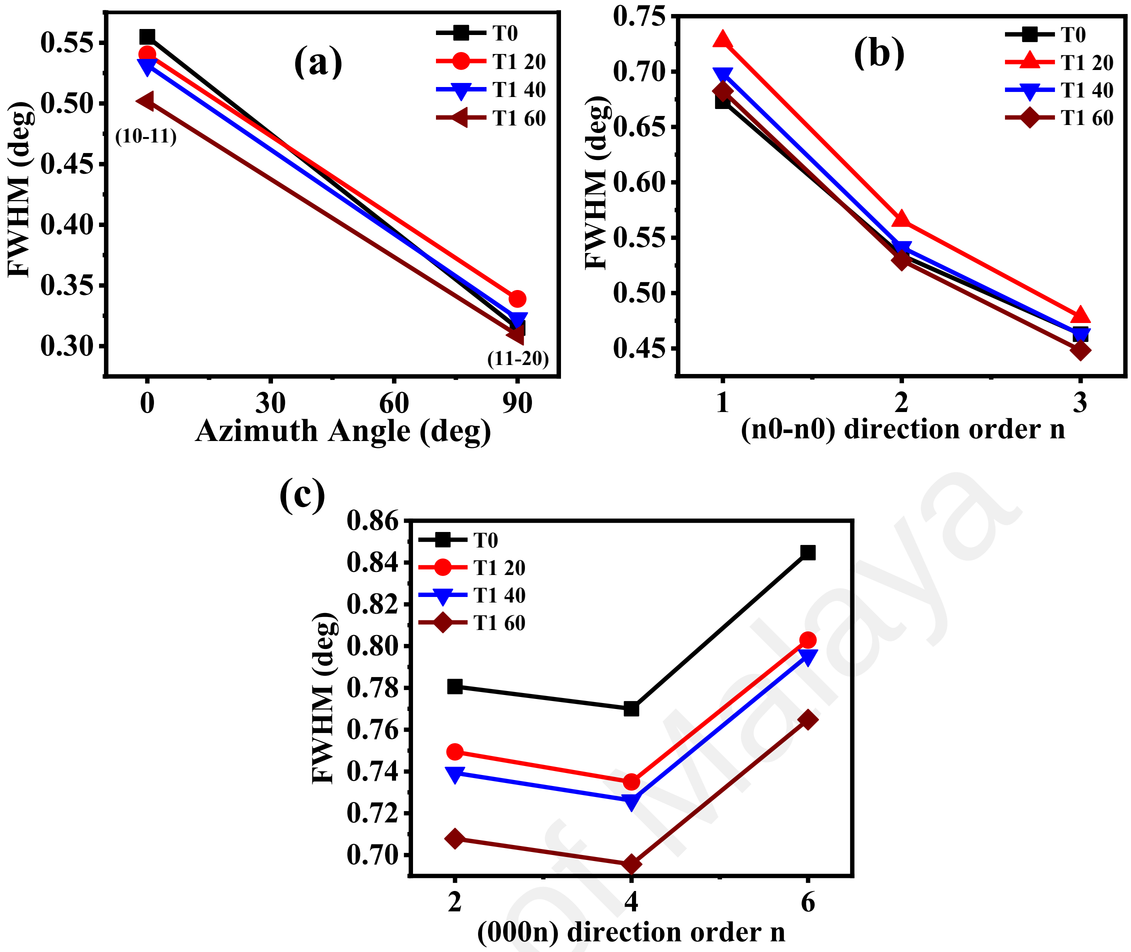

Figure 4.3: The Off-axis XRC (a) FWHM as a function of azimuthal angle (Φ), (b M-plane (n0-n0) FWHM with n equal to 1, 2, and 3, (c) C-plane (000n) FWHM with n equal to 2, 4, 6.

Further analyse of the crystal defects, namely PSFs, BSFs, and dislocations the Off-axis XRCs were implemented with various diffraction planes inclined respect to the (11-22) plane at a dissimilar azimuthal angle. As demonstrated in Figure 4.3(a), the XRC FWHM values of asymmetry scan for (10-11) and (11-20) diffraction plane narrowed with an increase of pairs I-SMAT employed increased. The T1 60 exerts significant narrowing of FWHMs for (10-11) and (11-20) diffraction planes elucidate the reduced density of perfect and PSFs, respectively (G. Zhao et al., 2016). These results were well correlated with the On-axis XRC FWHMs (Figure 4.2) proving an improvement of semi-polar (11-22) GaN crystal quality as the number of pairs increased.

The (n0-n0) planes XRC FWHMs with the diffraction order n increases from 1 to 3 were utilized to reveal the stacking faults formed within the semi-polar (11-22) GaN thin film. Figure 4.3(b) demonstrates the (n0-n0) planes XRCs showed a similar trend whereby T1 60 exhibits the lowest FWHMs. At first, T1 20 has broad (n0-n0) XRC FHWMs but become narrower as the number of pairs increases. Reports have shown that the (10-10) and (20-20) plane XRCs would correspond to the I_1- and I_2-type BSFs, respectively. The narrowing in the (10-10) and (20-20) plane would indicate BSFs densities reduction (Omar, Shuhaimi, et al., 2018; G. Zhao et al., 2016). The BSFs type I_1 is formed by either insertion or removal of a basal plane with a basal shear of 1/3<1-100> to reduce the fault energy (Zakharov et al., 2005). Furthermore, the BSFs type I_1 is also connected by a sessile Frank-Shockley dislocation with burger vector b = 1/6<20-23> and related with one PSFs by displacement vector b = 1/2<10-11>. Since the BSFs type I_1 have low fault energy it would be the most probable occurring type of stacking faults the growth process. As for BSFs type I_2, the basal plane slides by 1/3<1-100> in one part of the crystal generated by the dissociation of a perfect dislocation with b = 1/3<11-20> into two Shockley partials with b = 1/3<1-100> (Hsu, Su, Huang, Cheng, & Cheng, 2011).

Figure 4.3(c) displayed the Off-axis XRC FWHM along c-direction (000n) with n equal to 2,4 and 6. The narrowing of the (000n) XRC FWHM, on the other hand, would be owing to the partial and/or perfect dislocations (having a fault vector along c-axis) reduction (Sun et al., 2009). In Figure 4.3(c), the decrement of FWHMs value were observed as the number of pairs I-SMAT employed to increase and T1 60 has the highest reduction of dislocation down to 10% compared to T0. These results demonstrated the I-SMAT can effectively reduce the partial and/or perfect dislocation. A single ammonia treatment reported by Song et al. in 2013, also found that the treatment can effectively reduce dislocation density by selective etching at crystal defect sites (Song et al., 2013). Ammonia molecules at above 1000°C are highly reactive that promotes surface etching of the GaN epilayer (Hsu et al., 2011; Song et al., 2013). These NH_3 molecules can effectively etch defect-rich GaN sites compared to defect-free sites (Hsu et al., 2011; Sun et al., 2009). This is because the defect-rich site generated by underlying dislocation has lower bounded energy thus can be etched by NH_3 molecules at high temperature (Hsu et al., 2011; Sun et al., 2009).

The overall XRC results illustrated that the (10-11) and c-plane (000n) XRC FWHM diffraction plane are well correlated. While, XRC FWHM diffraction plane of (11-20) and m-plane (n0-n0) do not correlated with (10-11) and (000n). These explain that the I-SMAT techniques with implement of 1 SLM of NH_3 flux can effectively reduce the density of perfect dislocations because XRC FWHM of (10-11) and c-plane (000n) that are corresponded to partial and/or perfect dislocation, respectively. However, the PSFs, BSFs type I_1, and I_2 that are corresponded to (11-20), (10-10) and (20-20) XRC FWHM, respectively, has almost not affected or slightly increased by I-SMAT with 1 SLM of NH_3 flux. Nevertheless, the On-axis FWHM in Figure 4.2 showing crystal enhancement of semi-polar (11-22) Uid-GaN epilayer as the number of pair increases. Therefore, by correlating the result of XRC FWHM of Off- and On- axis, it suggests that the improvement of the crystal quality of the semi-polar (11-22) Uid-GaN epilayer via I-SMAT with NH_3 flux of 1 SLM is mainly contributed by reduction of perfect dislocation density.

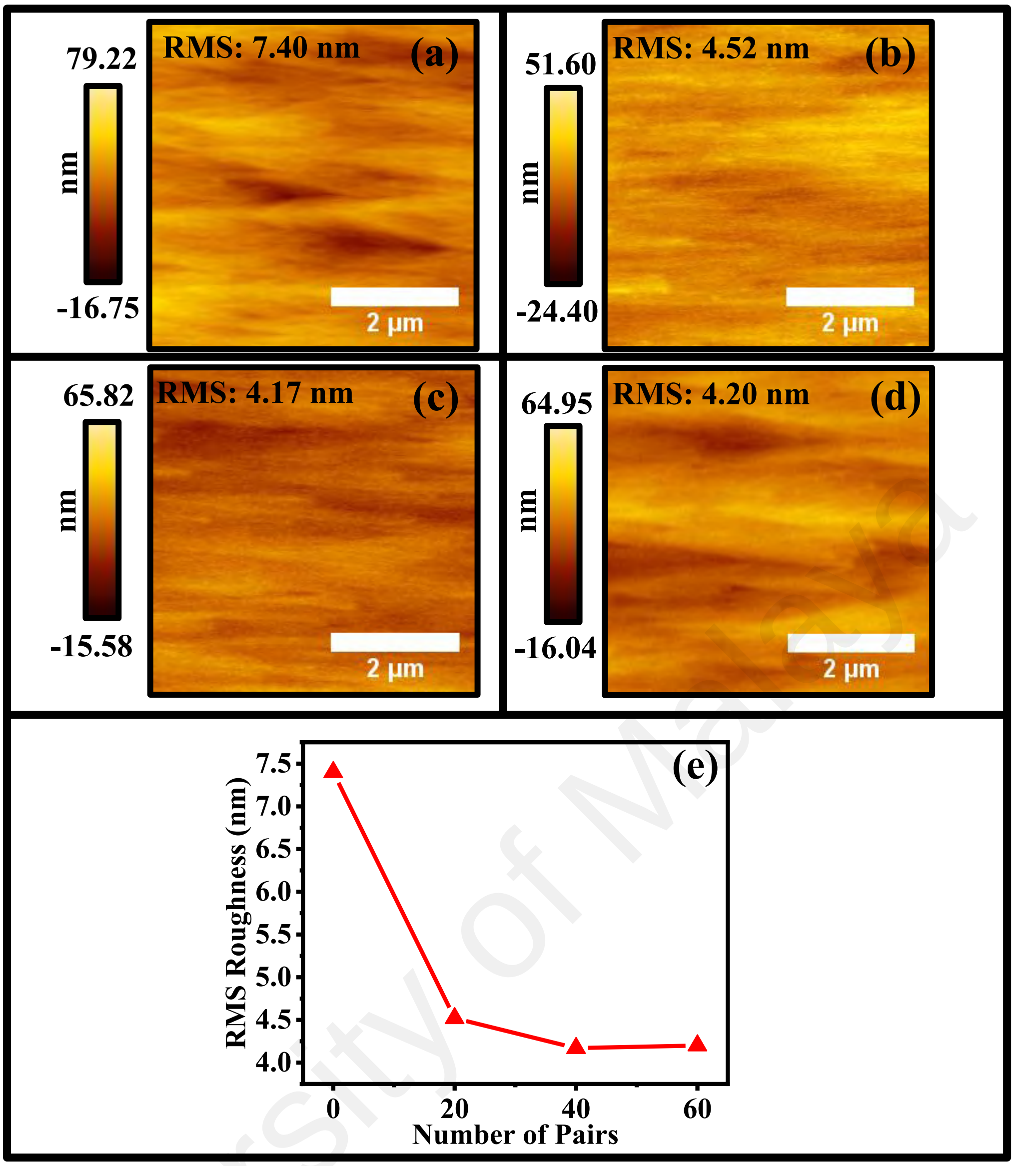

Figure 4.4: 5x5 μm^2 scan size AFM of (a) T0, (b)T1 20, (c)T1 40 and (d)T1 60. (e) The RMS roughness of all samples.

Figure 4.4(a)-(d) shows the 5x5 μm^2 scan size of four different pairs, confirming the presence of the arrowhead-like features. Such features may arise due to the short adatom diffusion length along [1-100] direction compared to [-1-123] (Ploch, Wernicke, Dinh, Pristovsek, & Kneissl, 2012). Based on the lattice structure of semi-polar (11-22) GaN, the surface atomic spacing [1-100] and [-1-123] are 5.53Å and 3.04Å, respectively. On the surface of T0, a large and clear arrowhead-like feature with the wide dark area that attributed to the formation of deep valleys was observed in Figure 4.4(a). This valley may originated by BSFs or dislocation that successfully propagates to the surface (Ahmad Makinudin et al., 2019). This valley features roughen the surface and provide more sites for oxidation. However, the density of the arrowhead-like features was observed to decrease upon utilizing the I-SMAT technique as depicted in Figure 4.4(a)-(c). As the number of I-SMAT employed increase, the density of arrowhead-like feature decrease resulting great reduction of surface roughness from 7.40 nm to 4.17 nm. By correlating the RMS roughness with On- and Off- axis XRC FWHM results, the T1 60 sample supposed to exhibit the smoothest surface as compared to all samples. However, from the AFM measurement, the T1 40 has lower RMS surface roughness then T1 60 by only 0.03 nm in which can be consider as identical. The decrement of RMS roughness elucidates the morphology and crystal enhance of semi-polar (11-22) GaN by reduction of stacking faults and dislocations density (Ahmad Makinudin et al., 2019; Song et al., 2013; Sun et al., 2009). Figure 4.4(e) illustrated the RMS roughness values progressively reduce as the number of pairs increase. In order to determine the causality of such a phenomenon, a 0.5×0.5 μm^2 scan AFM measurement was implemented to further analyze the morphological differences between the samples.

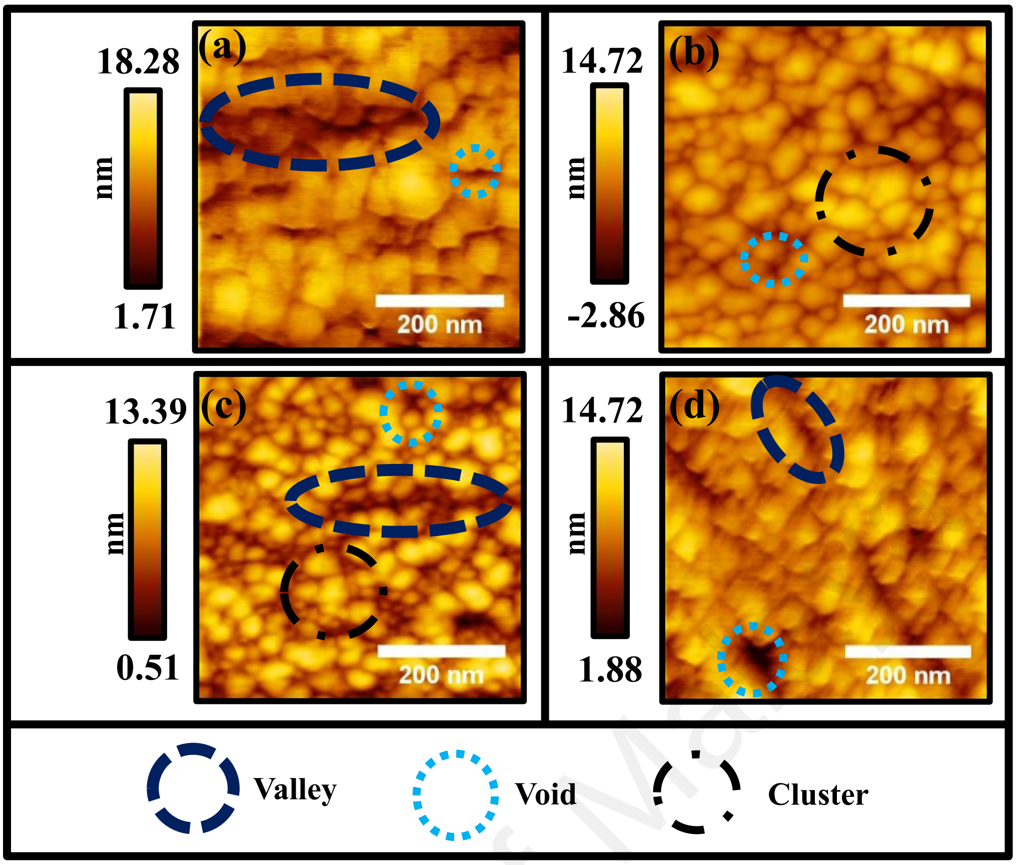

Figure 4.5: 0.5×0.5 μm^2 AFM images of (a) T0, (b) T1 20, (c) T1 40 and (d) T1 60.

In order to further evaluate the morphological properties, 0.5×0.5 μm^2 AFM scans were utilized. Figure 4.5 presents the high magnification of the AFM scans for all T1 samples. It can be observed that all the samples exhibit a terrace-like structure which is the common morphological properties of semi-polar (11-22) GaN (Omar, Shuhaimi, et al., 2018; Song et al., 2013; G. Zhao et al., 2016). However, sample T0 induced a large valley between the terraces (highlighted in the purple dashed circle) as shown in Figure 4.5(a). Upon implementation of I-SMAT, the terrace size becomes smaller and homogenous, resulting in a more compact arrangement. The T1 20 exhibit highly irregular distributes of the terraces size. Some of terraces were clustered. It is observed that the voided areas surrounded by clustered terrace create a valley as circle in Figure 4.5(b). In T1 40, the valley is elongated but the width is smaller forming an almost a straight line, and the atomic terrace structure is distributed randomly showing the terrace structure started to rearrange. As for T1 60, the valley width becomes very small forming straight line with the terrace structure is compactly distributed forming harmonious arrangement. It is reported that the valley width and void area were generated by extended crystal defects to the surface (Ahmad Makinudin et al., 2019). Therefore, these results reveal morphological structure enhancement in nanoscale from T0 to T1 60. It is worth noted that the AFM results are well correlated with the XRC measurement whereby the crystal quality is enhanced as the number of pairs I-SMAT implemented increase leading to morphological enhancement (Figure 4.2 and Figure 4.3).

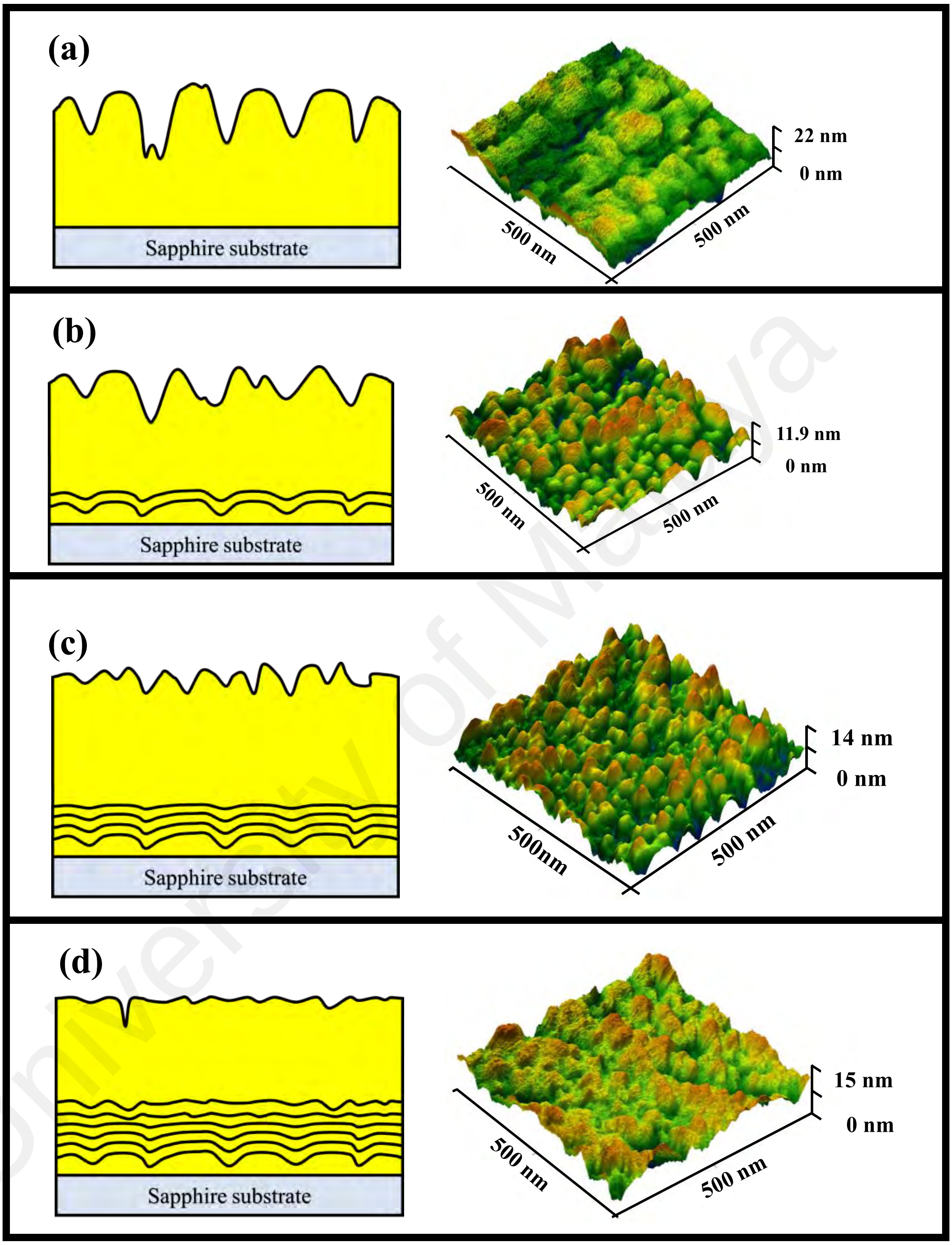

Figure 4.6: I-SMAT mechanism for (a) T0, (b) T1 20, (b) T1 40 and (c)T1 60.

Based on all results above, the crystal quality and the surface morphology are progressively enhanced as the number of pairs I-SMAT implemented increases. The On-and Off-axis XRC scans demonstrated a reduction density of BSFs and dislocations density that might due to thermal selective etched on defect sites at the underlying GaN layer (Song et al., 2013). At elevated temperature (>1000°C), NH_3 molecules at are highly reactive that would lead to surface etching of the GaN epilayer (Hsu et al., 2011; Song et al., 2013). These NH_3 molecules can effectively etch defect-rich GaN sites compared to defect-free sites (Hsu et al., 2011; Sun et al., 2009). This is because the defect-rich site generated by underlying dislocation has lower bounded energy thus it can be etched by NH_3 molecules at high temperature (Hsu et al., 2011; Sun et al., 2009). The combination of high temperature and partial pressure of NH_3, the low bonded GaN is highly to be etched by desorption of GaN to Ga and NH_3 {Hsu, 2011; Huang, 2017}. In addition, the NH_3 flux during the I-SMAT would induce the rearrangement of the terrace features due to the reactivity of NH_3 with the thin GaN layer. Thus, as number of pairs of I-SMAT employed increase, it induces a smoother underlying surface by the etching process that promotes crystal enhancement as depict in Figure 4.6 (a)-(c) (Ploch et al., 2010; Song et al., 2013).

4.2 Impact of I-SMAT Implemented with 2.3 SLM NH_3

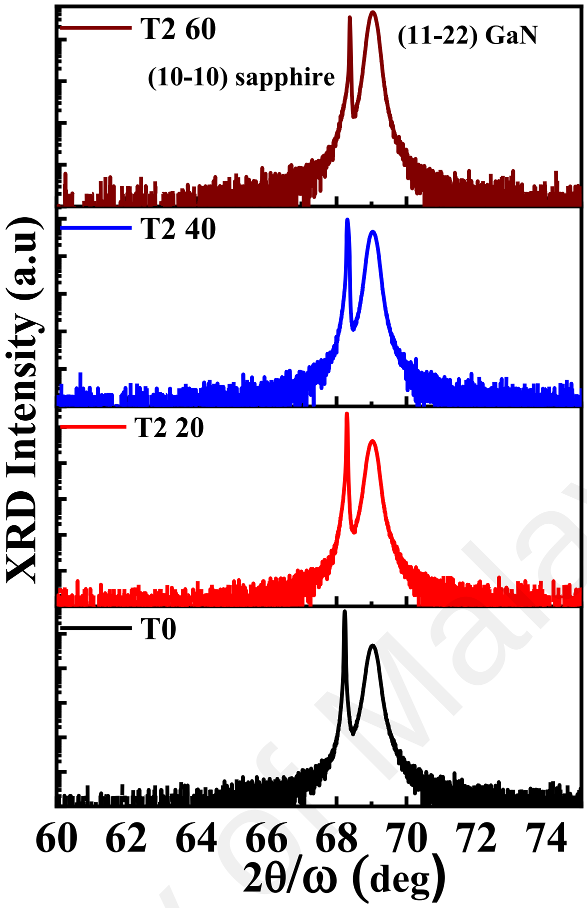

Figure 4.7: HR-XRD 2θ-ω scans of (11-22) Uid-GaN epitaxial layers grown on m-plane sapphire substrate for T2 with various pairs.

The HR-XRD 2θ-ω scans were implemented to T2 20, T2 40 and T2 60. In Figure 4.7, 68.2° and 69.0° diffraction peaks are corresponded to m-plane (10-10) sapphire substrate and semi-polar (11-22) GaN, respectively. As the HR-XRD 2θ-ω scans indicate all samples attained single crystalline (11-22) GaN on m-plane sapphire.

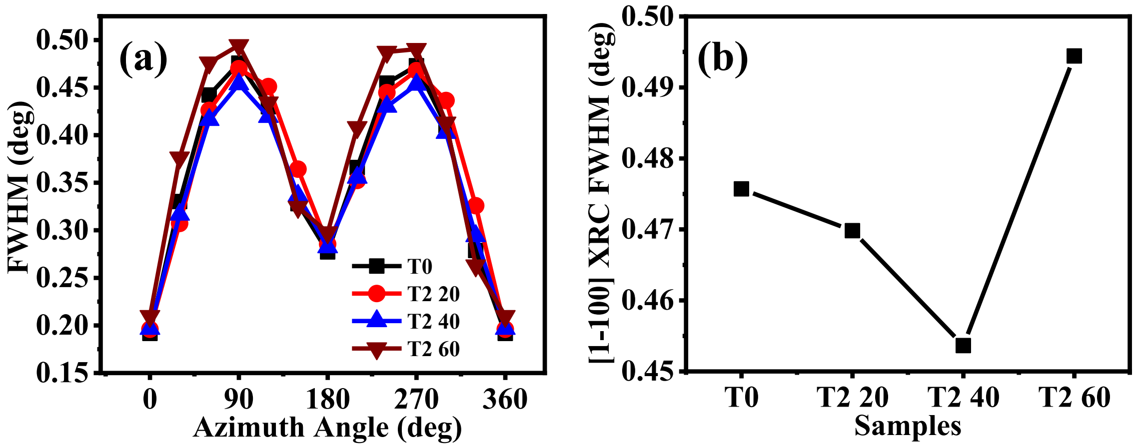

Figure 4.8: (a) On-axis XRCs FWHM of (11-22) GaN ω- scan as a function of azimuthal angle (Φ). (b) XRCs FWHM on [1-100] directions.

Figure 4.8 illustrated the On-axis analysis was taken for 20, 40 and 60 pairs with 2.3 SLM of NH_3 flux. As the previous result (T1), the FWHM values reduce as the pairs of I-SMAT implemented increase to 40. However, the FHWM of T2 60 is observed broader than T0 indicates crystal degradation as shown in Figure 4.8(b). The decrement of On-axis FWHM XRCs validates the reduction of crystal defects such as TDs, BSFs and PSFs (Frentrup et al., 2011; Zakharov et al., 2005; G. Zhao et al., 2016). This shows a threshold number of pairs I-SMAT implemented toward crystal enhancement reduce as the NH_3 flux applied is increased. Thus, T2 40 exhibits the highest crystal quality based on the On-axis analysis.

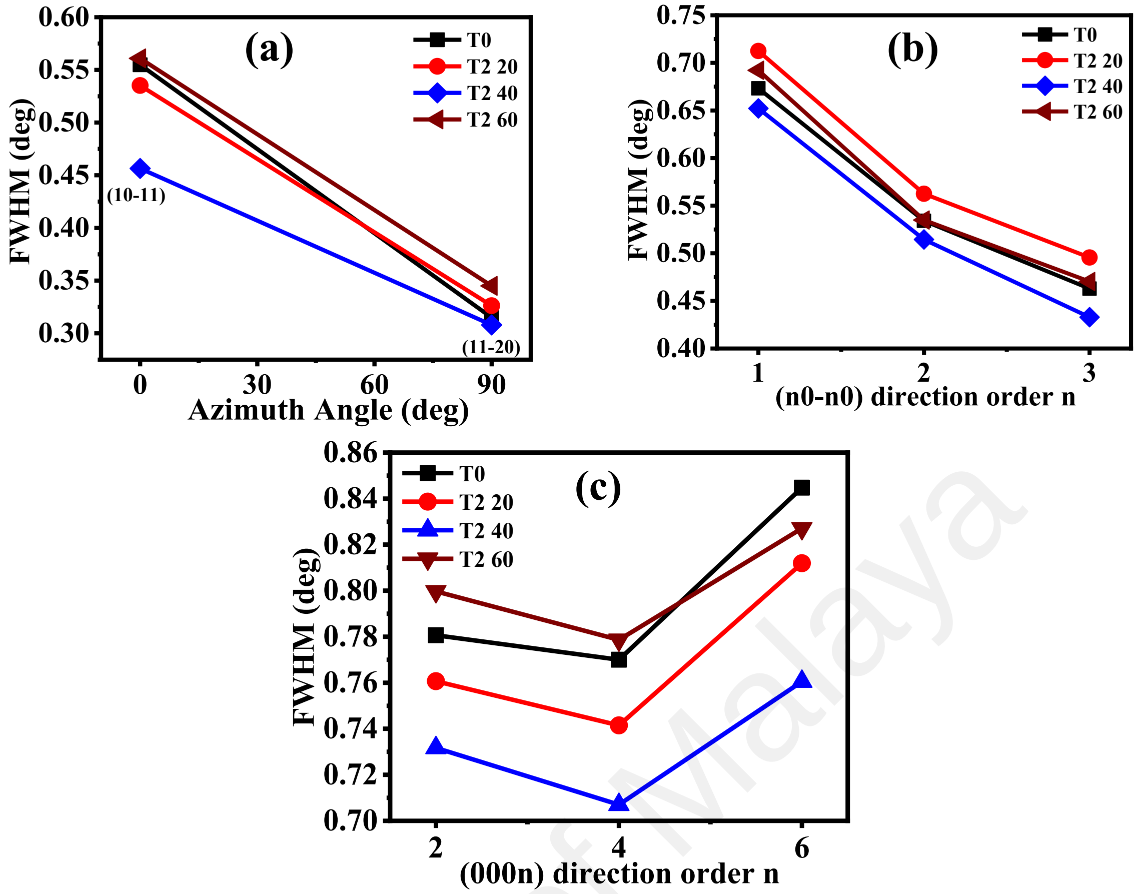

Figure 4.9: The Off-axis XRC (a) FWHM as a function of azimuthal angle (Φ), (b) M-plane (n0-n0) FWHM with n equal to 1, 2, and 3, (c) C-plane (000n) FWHM with n equal to 2, 4, 6.

The Off-axis XRCs was performed to all pairs of 2.3 SLM NH_3 flux to elucidate the micro defects in the semi-polar (11-22) GaN crystal. From the Figure 4.9 (a) , T2 40 exerts significant narrowing of the FWHMs for (10-11), and (11-20) diffraction planes elucidating the reduced density of perfect dislocations and PSFs, respectively (G. Zhao et al., 2016). This result correlates with On-axis XRCs FWHM which illustrated T2 40 greatly enhancement of semi-polar (11-22) GaN crystal. However, the T2 60 pairs is considered an excessive pair that can degrade the crystal quality of semi-polar (11-22) GaN.

The (n0-n0) planes XRCs in Figure 4.9(b) displayed the T2 40 has the lowest FWHM indicating T2 40 has the highest reduction of BSFs type I_1 and I_2 (G. Zhao et al., 2016). While the (000n) XRC scans in Figure 4.9(c), illustrated reduction of FWHM as the pair increases to 40 pairs owing to the reduction of partial and/or perfect dislocations (G. Zhao et al., 2016). Nevertheless, the T2 60 observed broadening of FWHM elucidating promotes of partial and/or perfect dislocation at excessive pairs (Omar, Shuhaimi, et al., 2018). Overall, Off-axis results display an optimum pair for certain NH_3 will enhance the semi-polar (11-22) GaN epilayer by effectively reduce the partial/perfect dislocation and the BSFs. Thus, T2 40 has the highest reduction of dislocation down to 9% compared to T0. However, upon implementing higher pairs of I-SMAT to 60 pairs, an increase in the FWHMs for the Off-axis diffraction plane was observed. These results demonstrated the I-SMAT can effectively reduce the partial and/or perfect dislocation at optimum ammonia flux and pairs. However, an excessive pair will worsen the crystal quality by adding more defects.

Illustrated in Figure 4.9(a)-(c), the (10-11) and c-plane (000n) XRC FWHM diffraction plane are well correlated, while not for XRC FWHM diffraction plane of (11-20) and m-plane (n0-n0). However, by comparing with all T1 samples, there is significant decrement of m-plane (n0-n0) XRC FWHM on T2 40 describing a great reduction of BSFs type I_1 and I_2 within the semi-polar (11-22) Uid-GaN epilayer. Is it reported that the BSFs can be terminated by PDs or folds of PSFs (Dasilva et al., 2010; Sun et al., 2009). This suggest the reduction of BSFs density in T2 40 is due to termination of BSFs by partial and/or PSFs propagate within the crystal. Therefore, the crystal quality of T2 40 is greatly enhanced by reduction of perfect dislocations, BSFs type I_1 and I_2.

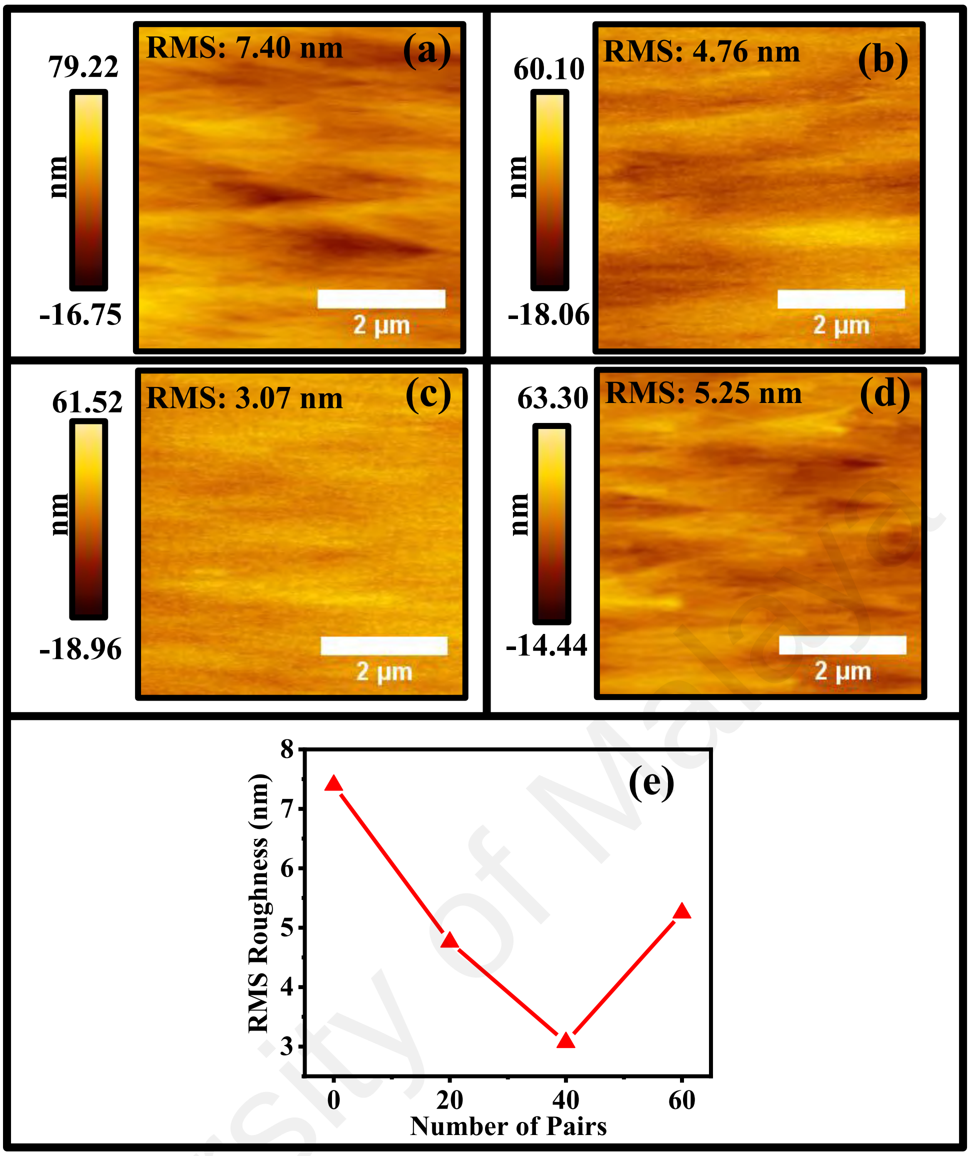

Figure 4.10: 5x5 µm scan size AFM of (a) T0, (b)T2 20, (c)T2 40 and (d)T2 60. (e) The RMS roughness of all samples.

Figure 4.10(a)-(d) represents the 5x5 µm scan size AFM images of 2.3 SLM of NH_3 flux with various pairs and T0 is given for comparison. The undulated arrowhead-like features depict in the AFM image significantly reduces as the pairs increase to 40 pairs which leads to a great reduction of surface roughness from 7.40 nm to 3.07 nm. However, upon increasing the number of pairs to 60, the undulated arrowhead-like features are more visible compared to T2 40 attributes to increment of RMS roughness to 5.25 nm. Nevertheless, these AFM analysis reveals a significant morphological enhancement by I-SMAT treatment at optimized NH_3 flux and pairs. It is noteworthy that the AFM results are well correlated with the On- and Off-axis XRC scan where the

BSFs and partial/perfect dislocations were reduced as the pair increases to 40 pairs (Ahmad Makinudin et al., 2019; Song et al., 2013; Sun et al., 2009). The RMS roughness value displayed in Figure 4.10(e) shows a similar pattern as [1-100] XRC FWHM in Figure 4.8(b). This proves the surface roughness was smoothened and roughen by the reduction and increment of crystal defects propagate to the surface, respectively. Thus, AFM measurement was implemented to further investigate the causality of such phenomenon and the morphological differences between the samples.

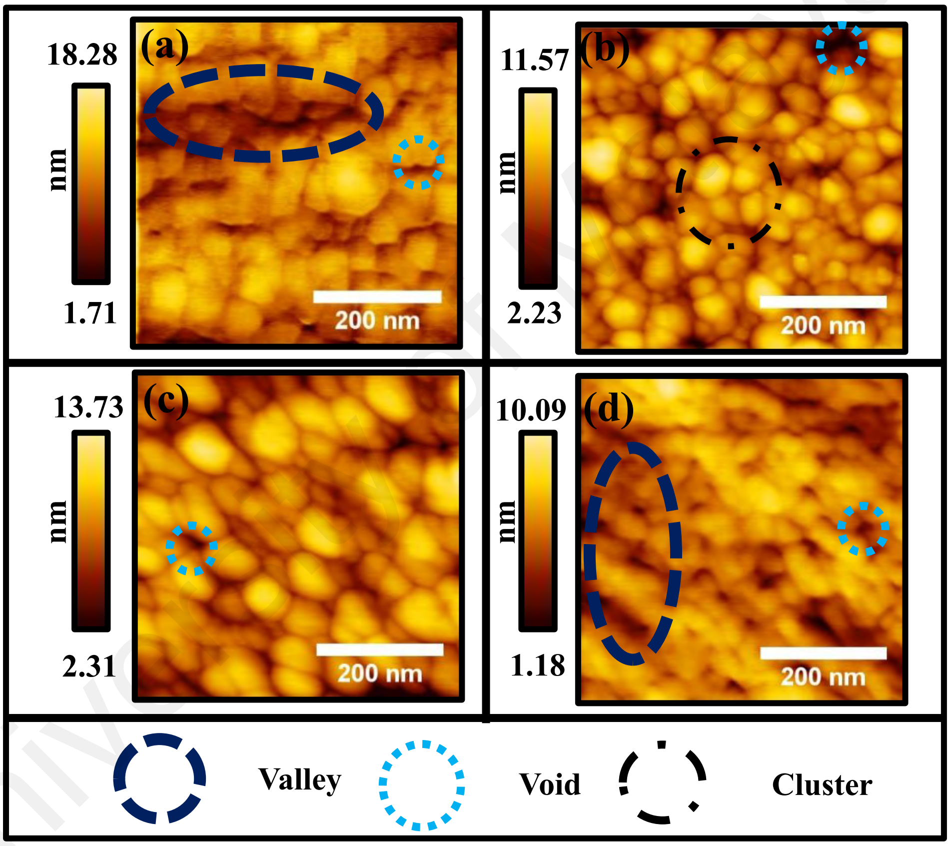

Figure 4.11: 0.5×0.5 µm^2 AFM images of (a) T0, (b) T2 20, (c) T2 40 and (d) T2 60.

In Figure 4.11(a)-(d), the 0.5×0.5 µm^2 AFM scans were implemented to further evaluate the morphological properties. As in the previous results, T0 exhibit a large valley between the terraces. A smaller and more compact terrace size was seen on all T2 samples surface attribute to the narrowing of the voided sizes especially T2 40. In T2 20, numbers of valley are started to absent on the surface, but a high density of voided sites is observed. Cluster atomic-terrace was also found showing surface structure started to rearrange. In T2 40, the voided area decreases with a compact yet orderly arranged terrace. However, in T2 60, the number of void spot increases and early stage of the valley formation are seen. The density of valley and void can elucidate the density of crystal defects in the thin film (Ahmad Makinudin et al., 2019). This describes the enhancement of nano-scale surface structure of semi-polar (11-22) GaN from T2 20 to T2 40 and surface degradation on T2 60 by termination and formation of crystal defect, respectively. These results are well correlated with the On- and Off-axis XRC scans (Figure 4.8 and Figure 4.9).

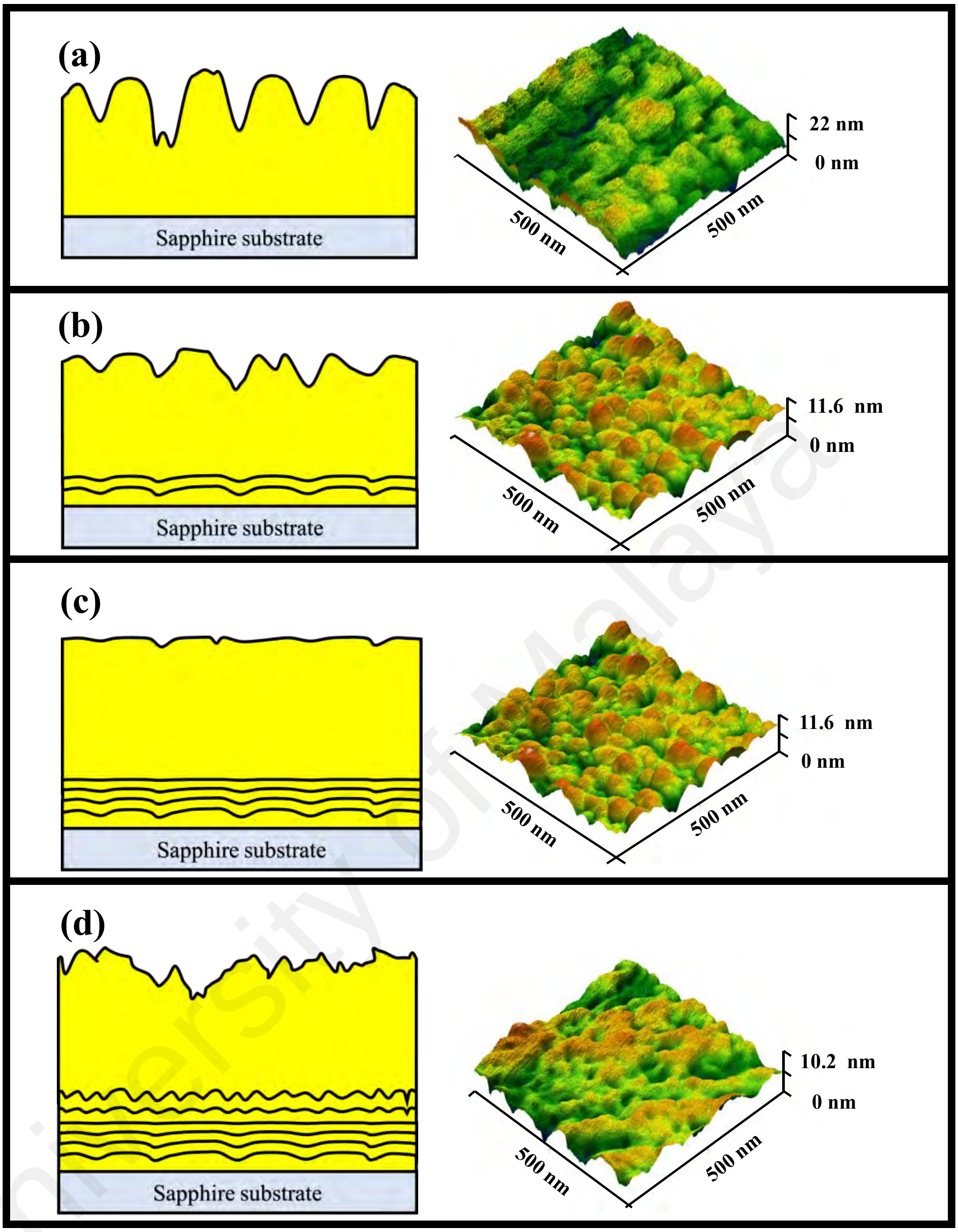

Figure 4.12: I-SMAT mechanism for (a) T0, (b) T2 20, (b) T2 40 and (c)T2 60.

The crystal quality and the surface morphology are enhanced as the number of pairs I-SMAT implemented increase but then degraded at 60 pairs. As discussed earlier, the crystal enhancement by I-SMAT was due to thermal selective etching on defect sites and surface smoothening at the underlying thin GaN layer (Ploch et al., 2010; Song et al., 2013). The ammonia molecules at elevated temperature (>1000°C) are highly reactive that promotes surface etching of the GaN epilayer (Hsu et al., 2011; Song et al., 2013). Therefore, NH_3 molecules etch defect-rich GaN sites due to its low bound energy (Hsu et al., 2011; Sun et al., 2009). In addition, a number of pairs of I-SMAT employed increase, it induces a smoother underlying surface by the etching process that promotes crystal enhancement as demonstrated in Figure 4.12(a)-(c) (Ploch et al., 2010; Song et al., 2013). However, at 60 pairs, the excessive ammonia flux may roughen most areas of the underlying layer promotes the increase of crystal defect that leads to surface degradation as demonstrated in Figure 4.12(d) (Ploch et al., 2010; Song et al., 2013). This explain despite high crystal defect density in the epilayer, that the implementation of I-SMAT cause better the surface morphology compare to without treatment. Nonetheless, by comparing with previous results, the T2 40 has higher crystal and morphological enhancement compared to T1 60. To further study the effect of NH_3 flux, higher NH_3 flux is implemented.

4.3 Impact of I-SMAT Implemented with 4 SLM NH$_3$

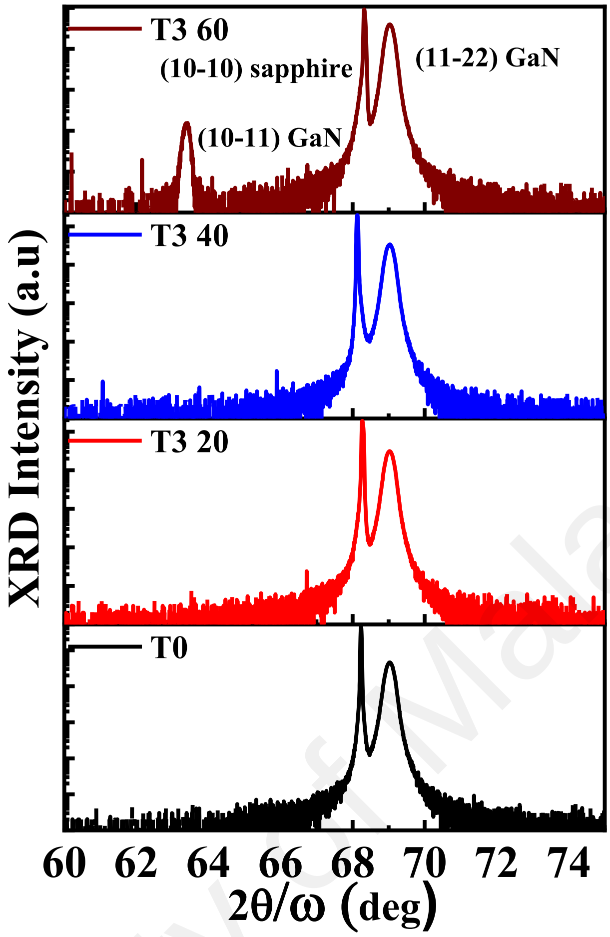

Figure 4.13: HR-XRD 2θ-ω scans of (11-22) Uid-GaN epitaxial layers grown on m-plane sapphire substrate for all pairs at 4 SLM.

In Figure 4.13, the HR-XRD 2θ-ω scans observed diffraction peaks at 63.4°, 68.2°, 69.0° attribute to semi-polar (10-13) GaN, m-plane (10-10) sapphire substrate, and semi-polar (11-22) GaN, respectively. All samples attained single crystalline (11-22) GaN on m-plane sapphire substrate except sample T3 60 which have a mixed phase of semi-polar (11-22) and (10-13) GaN. The low intensity of semi-polar (10-13) GaN at T3 60 ascribing it is a minor crystal surrounded with semi-polar (11-22) GaN crystal. Such occurrence facilitates the twinned-grain formation of semi-polar (11-22) and (10-13) in nanoscales resulting in a significant rise of surface roughness (Frentrup et al., 2011; Ploch et al., 2010).

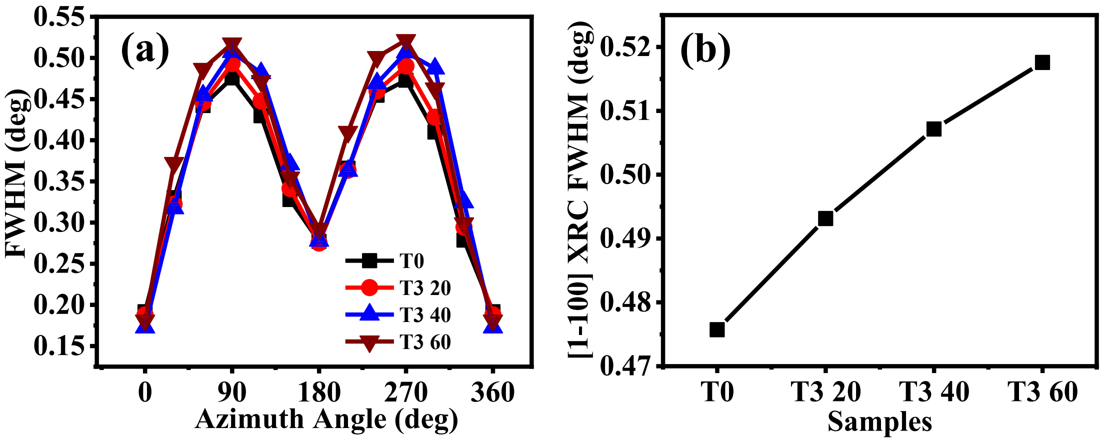

Figure 4.14: (a) On-axis XRCs FWHM of (11-22) GaN ω- scan as a function of azimuthal angle (Φ). (b) XRCs FWHM on [1-100] directions.

Figure 4.14 shows the On-axis XRC measurements with various azimuthal angle Φ were implemented to analyze the crystal quality of the sample. The On-axis analysis was taken from 0° to 360° with an interval of 30° whereas at 0° and 90°, the scanning direction is along (11-2-3) and (1-100), respectively. However, all samples exhibit the high broaden FWHM along [1-100] indicating an increased anisotropy resulted from the reduction of crystal quality. As illustrated in Figure 4.14(a) and (b), the FWHM for T3 sample increases as the pairs increase. This indicates the high implement of NH_3 flux leads to broadening the On-axis XRC FWHM values as the number of pairs increases. The broaden of On-axis FWHM is correlate with high dislocation densities and PSFs in the crystal (Frentrup et al., 2011; Zakharov et al., 2005; G. Zhao et al., 2016).

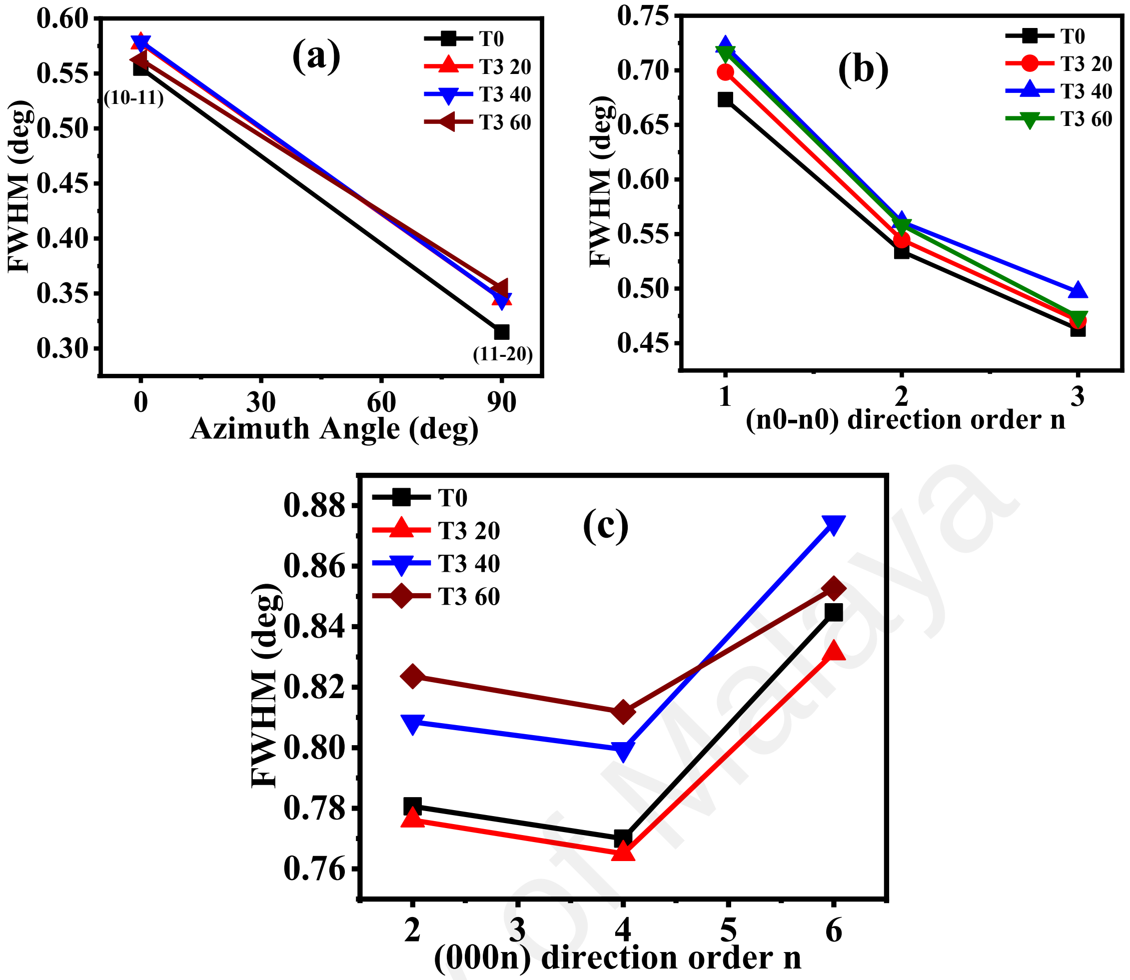

Figure 4.15: The Off-axis XRC (a) FWHM as a function of azimuthal angle (Φ), (b M-plane (n0-n0) FWHM with n equal to 1, 2, and 3, (c) C-plane (000n) FWHM with n equal to 2, 4, 6.

Further analyzing of the defects formed within the crystal, the Off-axis XRCs was implemented with various diffraction planes inclined respect to the (11-22) plane. From the Figure 4.15 (a), as pairs increase, the FWHMs for (10-11) and (11-20) diffraction planes significant broaden elucidating the reduced density of perfect dislocations and PSFs, respectively (G. Zhao et al., 2016).

The stacking faults in the crystal was analysed via the (n0-n0) planes XRCs with the diffraction order n increases from 1 to 3 was implemented respectively to the (11-22) plane. As in Figure 4.15(b), the FWHM of (n0-n0) plane broaden as the pairs increase illustrated it is well correlated with On-axis scans. The XRC FWHM for (000n) scan shows sample T3 20 has the narrower FWHM compared to T0 owing reduction of the partial and/or perfect dislocation. Nonetheless, overall results show T3 samples will lead to crystal degradation. This demonstrates a high NH_3 will worsen the semi-polar (11-22) GaN epilayer. This indicates the excessive ammonia flux and pairs of I-SMAT broaden the FWHM. Such phenomenon relates well with the On-axis measurements as well as the surface observations whereby the increase in NH_3 flux would exert an excessive etching of the surface resulting in crystal quality degradation.

Unlike I-SMAT with 1 and 2.3 SLM of NH_3 flux, all XRC results (On- and Off-axis) of T3 samples are correlated except for c-plane (000n) XRC FWHM. The c-plane (000n) XRC FWHM shows there is a reduction of PDs by I-SMAT with 4 SLM of NH_3 flux on T3 20. However, the On-axis XRC reveals a crystal degradation of T3 20 compared to T0 by the increase of perfect dislocation, PSFs, BSFs type I_1 and I_2.

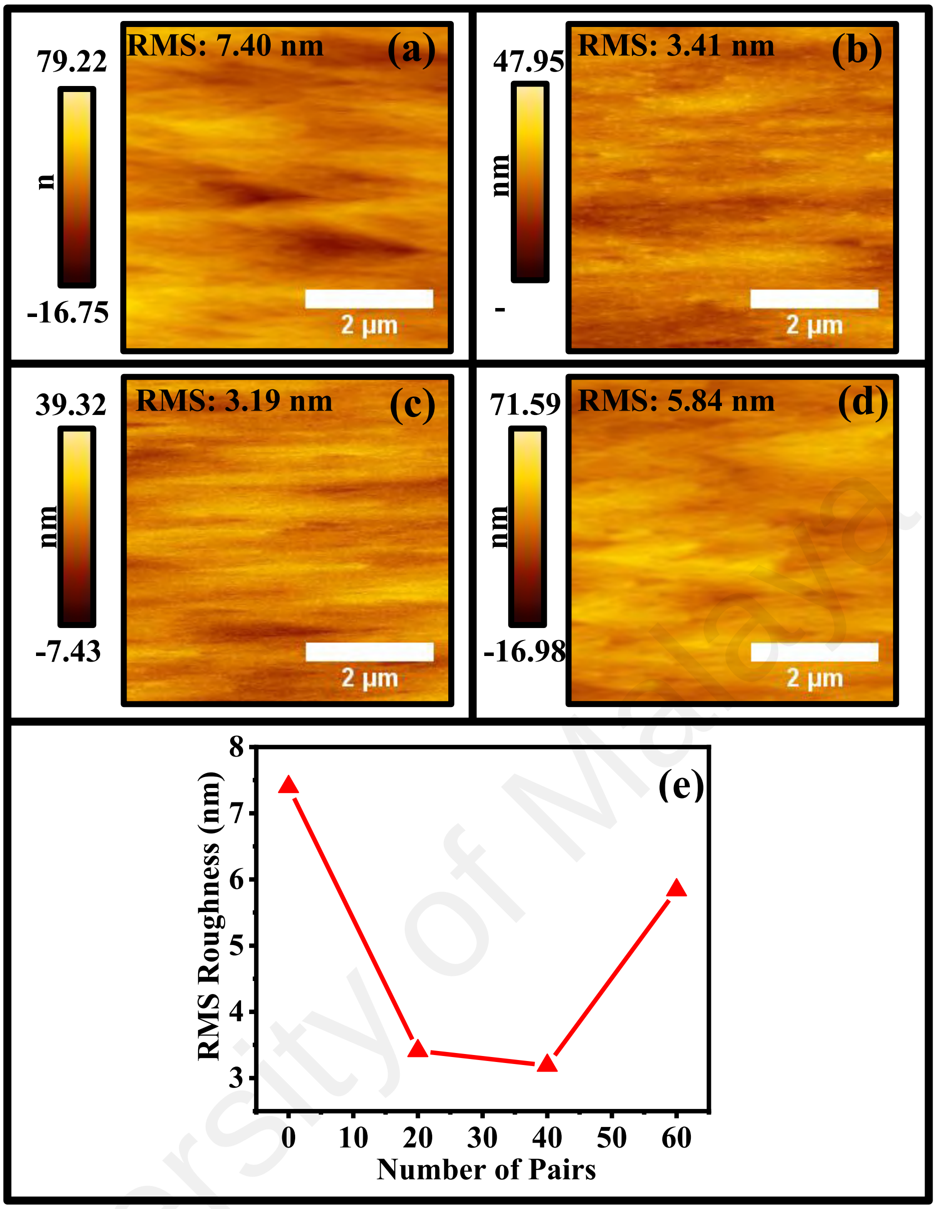

Figure 4.16: 5x5 µm^2 scan size AFM of (a) T0, (b) T3 20, (c) T3 40 and (d) T3 60. The RMS roughness of all samples.

The surface morphology of 20, 40, and 60 pairs at 4 SLM of NH_3 was analyzed by AFM measurement over 5x5 µm scan size as displayed in Figure 4.16(a)–(d) and T0 is illustrated for direct comparison. In Figure 4.16(b) and (c), the undulated arrowhead-like features for the common semi-polar (11-22) epitaxial layer on m-plane sapphire were reduced as the pairs increase to 40 pairs resulting reduction of surface roughness to 3.19 nm. Whilst, these features were larger upon increasing the number of pairs to 60 resulting an increase of RMS roughness to 5.84 nm as shown in Figure 4.16(d). As compare to sample T1 and T2, the RMS roughness does not well correlate with crystallinity for sample T3. This reveals that the I-SMAT treatment able to significantly smooth the surface of semi-polar (11-22) epilayer even with high crystal defects. Based on literature, such result can be obtained by smoothing the underlying thin GaN layer {Zhou, 2015; Smith, 2004; He, 2006; Chugh, 2017}.

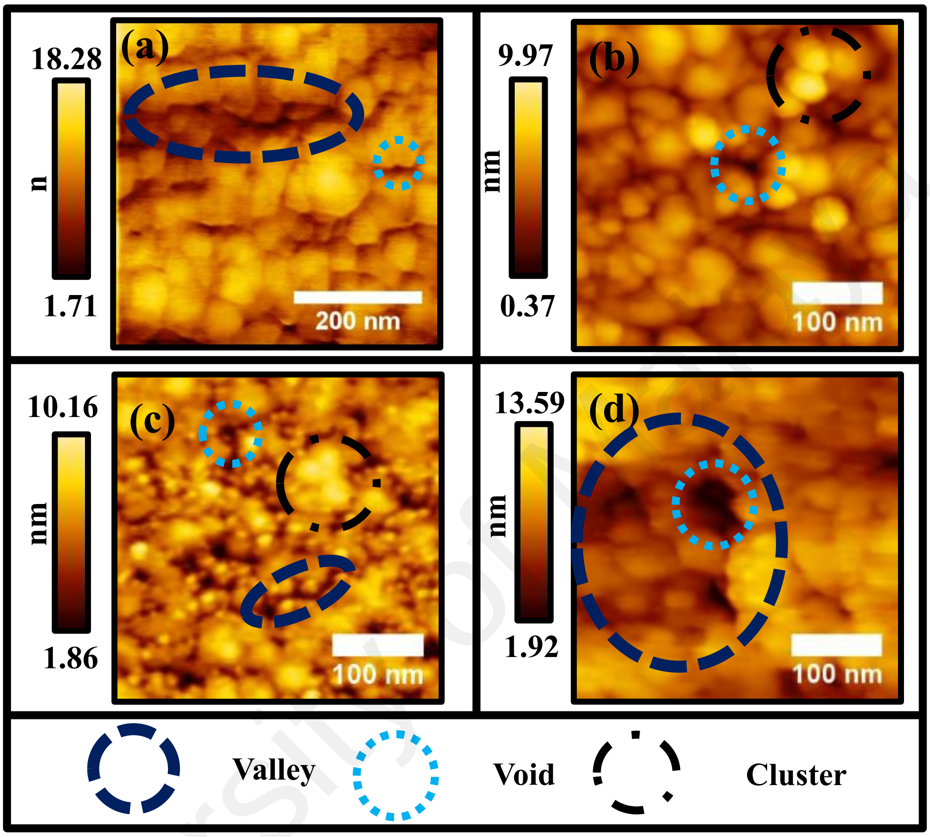

Figure 4.17: 0.5x0.5 µm^2 scan size AFM image of (a) T0, (b) T3 20, (c) T3 40, and (d) T3 60.

The morphological properties were further analyzed by utilizing 0.5×0.5 µm^2 AFM scans as shown in Figure 4.17(a)–(d). The typical terrace-like structure of semi-polar (11-22) GaN were exhibit on all samples (Omar, Shuhaimi, et al., 2018; Song et al., 2013; G. Zhao et al., 2016). From Figure 4.17, all T3 samples exhibit grain size inhomogeneity showing a sign of surface degradation. The T3 20 surface morphology is almost similar to T2 40 depicted in Figure 4.11(c) but has a more void spot. A cluster arrangement of atomic terrace structure showing terrace structure starts to disarrange. In T3 40, the voided density is increase and small valleys started to generate. Lastly, the large and deep valley is formed in T3 60 with void sites inside it (Figure 4.17(d)). This large valley may form from the combination of voids (Ahmad Makinudin et al., 2019).

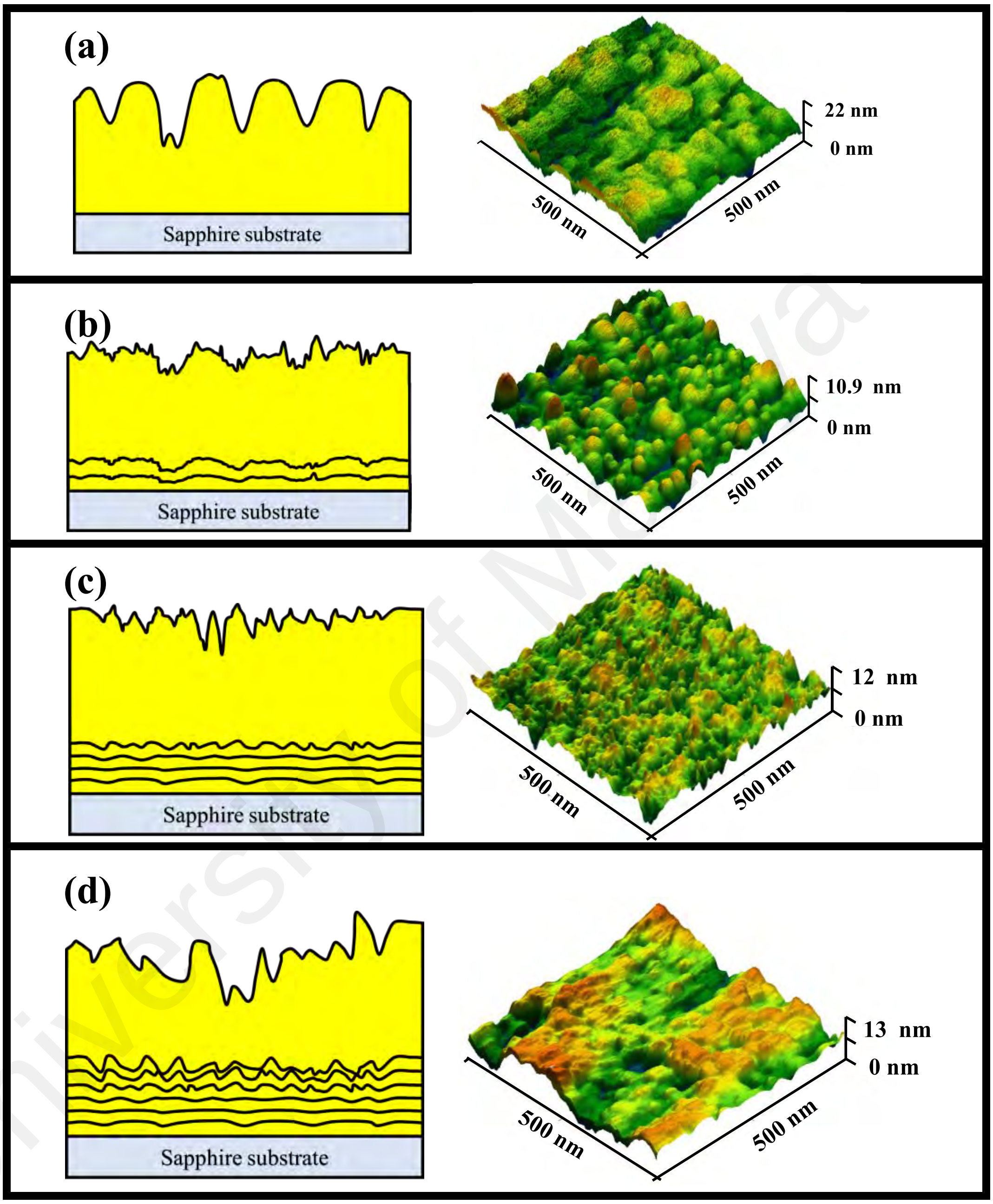

Figure 4.18: I-SMAT mechanism for (a) T0, (b) T3 20, (c) T3 40 and (d)T3 60.

Comparing with lower NH_3 flux (T1 and T2), T3 sample morphology degrades upon a higher number of pairs is implemented. This is well correlated with XRC results whereby the crystal quality of semi-polar (11-22) epitaxial layer reduces from T3 20 to T3 60 due to rise of PSFs and BSFs density. The formation of rough Uid- GaN surface may due to rough thin-GaN surface at the underlying layer by excessive etching of ammonia flux (Ploch et al., 2010; Song et al., 2013). At elevated temperature (>1000°C), NH_3 molecules are highly reactive that promote surface etching of the GaN epilayer (Hsu et al., 2011; Song et al., 2013). These NH_3 molecules can effectively etch defect-rich GaN sites compared to defect-free sites leading to crystal enhancement (Hsu et al., 2011; Sun et al., 2009). However, excessive NH_3 flux can excessively etch thin GaN causing rough surface. The surface roughness of the underlying layer is worsened as more pair of I-SMAT is employed as demonstrated in Figure 4.18(a)-(c). This rough underlying surface will promote the crystal defect leading to crystal and morphology degradation (Ploch et al., 2010; Song et al., 2013). Despite of having a highly crystal defect density in sample T3 40 and T3 60, the embedment of rough underlying surface can smoothing the Uid-GaN surface by providing more sites for Ga and N adsorption {Zhou, 2015}. An increase of Ga and N adsorption sites will increase the surface kinetic that attributes to smoother surface roughness {Zhou, 2015; Smith, 2004; He, 2006; Chugh, 2017}

4.4 Summary

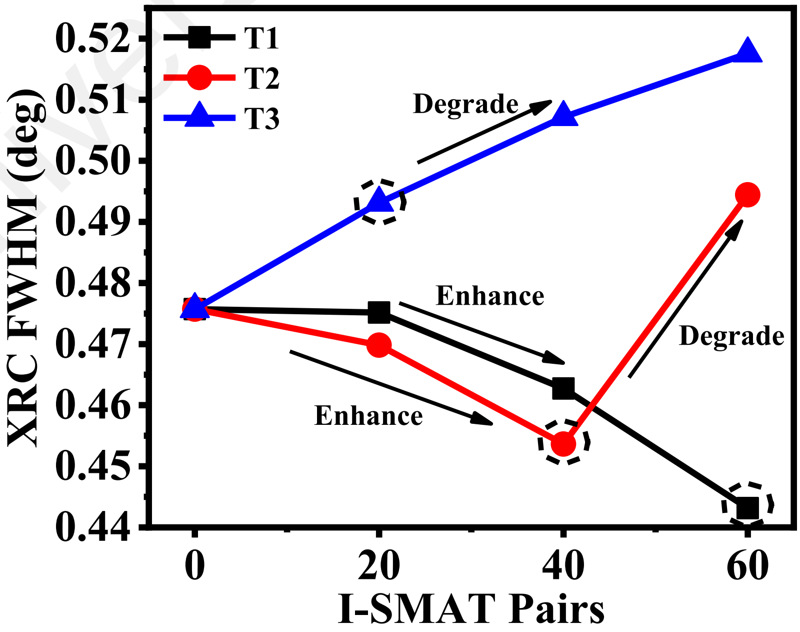

Figure 4.19: The [1-100] XRC FWHM for all samples.

In order to generally summarize the impact of the crystallinity of all samples, the [1-100] XRCs FWHM of all samples are plotted in Figure 4.19. As demonstrated in Figure 4.19, the values of the FWHM for T1 samples progressively decrease as the number of pair increases. This attribute to the reduction of BSFs type I_1 and partial or/and perfect dislocations as discussed earlier. As NH_3 increases to 2.3 SLM (T2), the XRC FWHM value reduces upon increasing the number of pairs to 40 but broaden at 60 pairs. This pattern illustrated I-SMAT with intermediate NH_3 flux required intermediate pairs for improving the crystal quality of semi-polar (11-22) GaN while excessive pair such as 60 pairs degrade. At higher NH_3 flux (T3), the XRC FWHM become more broaden with the increase of pairs. This elucidates excessive NH_3 flux promotes crystal degradation with the increment of pairs. To further investigate the optimum I-SMAT parameter for crystal enhancement, the best of crystal quality of each NH_3 flux is compared using On- and Off-axis XRCs FHWM. The best of each NH_3 flux are circled with a black dashed line. The best for each NH_3 flux is T1 60, T2 40, and T3 20.

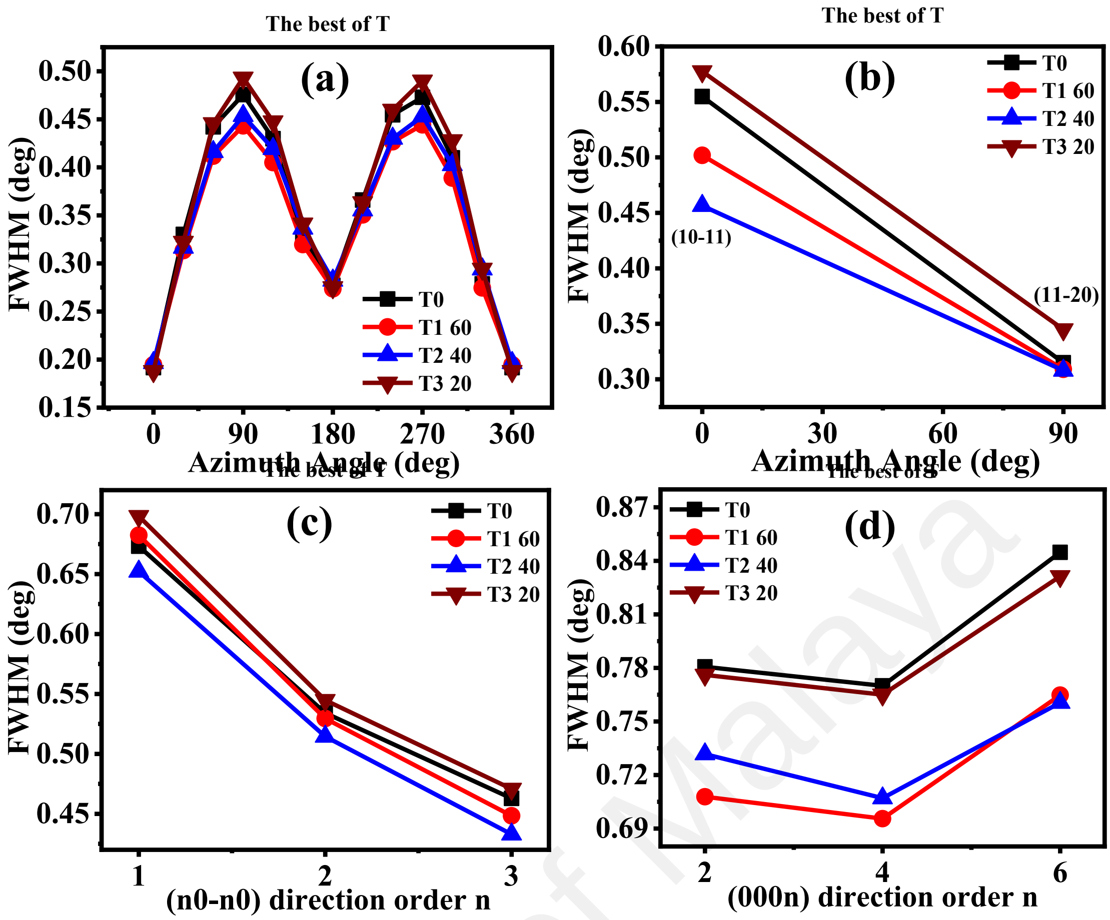

Figure 4.20: (a) On-axis XRCs FWHM of (11-22) GaN ω- scan as a function of azimuthal angle (Φ). The Off-axis XRC (b) FWHM as a function of azimuthal angle (Φ), (c) M-plane (n0-n0) FWHM with n equal to 1, 2, and 3, and (d) C-plane (000n) FWHM with n equal to 2, 4, 6.

To find an optimum I-SMAT parameter for crystal quality enhancement, the On- and Off-Axis XRCs FWHM of T0, T1 60, T2 40 and T3 20 are compared in Figure 4.20(a)–(d). As shown in Figure 4.20(a), the scan at 90° (direction is along (1-100), T1 60 exhibits the lowest value XRC FWHMs value follow by T2 40, T0 and T3 20. As stated before, the narrow of [1-100] XRC FWHM is direct correspond to the reduction of PSFs and partial/perfect dislocation. Whilst, the T2 40 On-axis XRC FWHM is nearly equivalent to T1 60 showing both crystal qualities are generally almost equal. Thus, the Off-axis XRCs FWHM is required to determine the lowest crystal defect reduction by I-SMAT.

The Off-Axis scan displayed in Figure 4.20(b) shows the T2 40 has the narrowest FWHM values, especially at (10-11) plane scans reduce approximately ~17.72%. The decrement of (10-11) and (11-20) FWHM diffraction planes are attributed to the reduced density of perfect dislocations and PSFs, respectively. A similar result is observed on the (n0-n0) diffraction plane scans elucidating T2 40 has the lowest FWHM value follow by T1 60. This (n0-n0) XRC FWHMs is correlated to BSFs type I and type II (Omar, Shuhaimi, et al., 2018; G. Zhao et al., 2016). The Off-axis XRC FWHMs along c-plane direction scans in Figure 4.20(d) illustrated a significant reduction FWHMs value by approximately ~10% and 9% for T1 60 and T2 40. These reductions are corresponding to a low density of BSFs that connected to PDs (Sun et al., 2009). As discussed earlier, BSFs type I_1 can be terminated by PDs and folded by PSFs. From the Off-axis XRC FWHMs measurement, T2 40 attained a higher reduction density of perfect and PSFs as compared to T1 60 elucidates T2 40 has better reduction of BSFs type I_1 density. Nevertheless, the overall Off-axis XRCs FWHM scan indicates T2 40 has the best semi-polar (11-22) GaN crystal quality. This can be further supported by the AFM measurement whereby T2 40 exhibits the lowest RMS roughness of 3.07 nm (58.51% RMS roughness reduction) as displayed in Table 4.2.

Table 4.2: RMS roughness with percentage different of T1 60, T2 40 and T3 60 relative to T0.

Sample	**RMS Roughness (nm)**	**Percentage different of RMS Roughness relative to T0,** $\left(\frac{\mathbf{7.40} - \boldsymbol{RMS\ Roughness}}{\mathbf{7.40}} \times \mathbf{100\%}\right)$
T1 60	4.20	43.24
T2 40	3.07	58.51
T3 20	3.41	53.92

CHAPTER 5: CONCLUSION

5.1 Conclusion

In this dissertation, we addressed the difficulty and problems faced in the growth of semi-polar (11-22) GaN. High crystal defect namely PSFs, BSFs, partial and perfect dislocation are major issues in semi-polar (11-22) GaN epitaxy. As the GaN lattice is tilted by 58.3° respective to c-plane, the stacking faults, and dislocation generated in the lattice propagate to the surface promoting surface degradation. Tremendous techniques have been introduced to overcome these obstacles. However, most of these popular techniques either required additional expensive equipment, time consuming or small-scale production. Therefore, it is important to find simple semi-polar (11-22) GaN epitaxy techniques to meet industrial needs and more economical. So far, the simplest crystal enhancement of semi-polar (11-22) GaN technique is ammonia treatment introduced by Song et al. (Song et al., 2013). This great work has shown ammonia treatment can effectively terminate defect at the underlying layer. Thus, the surface is simultaneously enhanced as the crystal is enhanced. However, the type of crystal defect reduces, and surface structure mechanism was not discussed in detail. Moreover, we believe this technique can be improvised to be more effective.

Inspired by ammonia treatment, we introduced In-Situ Multiple Ammonia Treatment (I-SMAT). In this method, thin GaN film (20nm) that has been treated by NH_3 flux is deposited multiple times and followed by the growth of a 4.5µm thick Uid-GaN epilayer. In this work, we implemented 20,40 and 60 pairs of I-SMAT with various NH_3 flux of 1, 2.3 and 4 SLM. Each sample was named in a simple term as shown in Table 4.1. Based on XRD measurement, it is found that this treatment can effectively terminate various crystal defects. These crystal defects are BSFs type I_1, I_2, PSFs, partial and perfect dislocations. From Off-axis XRC FWHMs, these defects progressively reduce as the number of I-SMAT pairs implemented increases from T0 to T2 40. The

Off-axis XRC FWHM for diffraction plane of (10-11) illustrated decrement of perfect dislocations about 17.72% as compared to T0. The enhancement of crystal quality by I-SMAT was contributed by the significant reduction of partial and/or perfect dislocation whereby the (000n) XRC FWHM show reduction about ~10% as compared with bare GaN. The enhancement of crystal quality of semi-polar (11-22) GaN simultaneously enhance its surface structure. Arrowhead-like features corresponding to the defect densities were observed to recede as deformation and rearrangement of the terrace step to a uniformly distributed arrangement was observed with the use of 1 SLM of NH_3. A significant reduction of RMS roughness about 58% was attained by the I-SMAT approach. Such occurrence is seen to originate from the crystal quality enhancement where it is presumed that the use of selective-area etching would discard the dislocation propagation. In comparison with the single ammonia treatment introduced by Song, et al., our results are greater in terms of crystal quality and morphology whereby their [1-100] XRC FWHM and RMS roughness are 828 arsec and 23 nm while in this work is 673 arsec and 3.07 nm, respectively. Thus, I-SMAT is the simplest technique that can be utilized for the enhancement of semi-polar (11-22) GaN epitaxial layer grown on m-plane (10-10) sapphire substrate.

5.2 Future Works

Further optimization on I-SMAT can be done to make it more efficient toward crystal and morphological enhancement of semi-polar (11-22) GaN epitaxial layer grown on m-plane sapphire substrate. For future work, the effect of semi-polar (11-22) GaN epitaxial layer with a function of time of NH_3 purge can be studied to find a greater crystal enhancement. Moreover, the thickness of the treated underlying GaN layer can be varied during I-SMAT for further defect reduction.

REFERENCES

Agrawal, M., Radhakrishnan, K., Dharmarasu, N., & Pramana, S. S. (2015). Effect of III/V ratio on the polarity of AlN and GaN layers grown in the metal rich growth regime on Si (111) by plasma assisted molecular beam epitaxy. *Japanese Journal of Applied Physics*, *54*(6), Article#065701.

Ahmad Makinudin, A. H., Omar, A. Z., Anuar, A., Bakar, A. S. A., DenBaars, S. P., & Supangat, A. (2019). Impact of a Strained Periodic Multilayer on the Surface and Crystal Quality of a Semipolar (11–22) GaN Template. *Crystal Growth & Design*, *19*(11), 6092-6099.

Amano, H., Baines, Y., Beam, E., Borga, M., Bouchet, T., Chalker, P. R., ... De Santi, C. (2018). The 2018 GaN power electronics roadmap. *Journal of Physics D: Applied Physics*, *51*(16), Article#163001.

Amano, H., Sawaki, N., Akasaki, I., & Toyoda, Y. (1986). Metalorganic vapor phase epitaxial growth of a high quality GaN film using an AlN buffer layer. *Applied Physics Letters*, *48*(5), 353-355.

Chen, J., Han, X., Huang, P., Chen, W., Liang, J., Zhong, C., ... Zhang, B. (2017). Schottky performance variation on r-plane and c-plane of GaN micro truncated-pyramid grown by selective area MOCVD. *Materials Science in Semiconductor Processing*, *63*, 248-252.

Das, A., Magalhaes, S., Kotsar, Y., Kandaswamy, P. K., Gayral, B., Lorenz, K., ... Monroy, E. (2010). Indium kinetics during the plasma-assisted molecular beam epitaxy of semipolar (11− 22) InGaN layers. *Applied Physics Letters*, *96*(18), Article#181907.

Dasilva, Y. A. R., Chauvat, M. P., Ruterana, P., Lahourcade, L., Monroy, E., & Nataf, G. (2010). Defect structure in heteroepitaxial semipolar (11-22)(Ga, Al) N. *Journal of Physics: Condensed Matter*, *22*(35), Article#355802.

Frentrup, M., Ploch, S., Pristovsek, M., & Kneissl, M. (2011). Crystal orientation of GaN layers on (1010) m-plane sapphire. *Physica Status Solidi (b)*, *248*(3), 583-587.

Fujito, K., Kubo, S., & Fujimura, I. (2009). Development of bulk GaN crystals and nonpolar/semipolar substrates by HVPE. *MRS Bulletin*, *34*(5), 313-317.

Funato, M., Ueda, M., Kawakami, Y., Narukawa, Y., Kosugi, T., Takahashi, M., & Mukai, T. (2006). Blue, green, and amber InGaN/GaN light-emitting diodes on semipolar {11-22} GaN bulk substrates. *Japanese Journal of Applied Physics*, *45*(7L), L659-L662.

Hangleiter, A., Hitzel, F., Netzel, C., Fuhrmann, D., Rossow, U., Ade, G., & Hinze, P. (2005). Suppression of nonradiative recombination by V-shaped pits in GaInN/GaN quantum wells produces a large increase in the light emission efficiency. *Physical Review Letters*, *95*(12), Article#127402.

Hsu, H. C., Su, Y. K., Huang, S. J., Cheng, S. H., & Cheng, C. Y. (2011). Improvement of a-plane GaN crystalline quality by overgrowth of in situ etched GaN template. *Journal of Crystal Growth*, *315*(1), 192-195.

Jeong, J., Jang, J., Hwang, J., Jung, C., Kim, J., Lee, K., ... Nam, O. (2013). Improved performance of semi-polar (11-22) GaN-based light-emitting diodes grown on SiNx interlayer. *Journal of Crystal Growth*, *370*, 114-119.

Konar, A., Verma, A., Fang, T., Zhao, P., Jana, R., & Jena, D. (2012). Charge transport in non-polar and semi-polar III-V nitride heterostructures. *Semiconductor Science and Technology*, *27*(2), Article#024018.

Koukitu, A., Takahashi, N., & Seki, H. (1997). Thermodynamic study on metalorganic vapor-phase epitaxial growth of group III nitrides. *Japanese Journal of Applied Physics*, *36*(9A), L1136-L1138.

Lin, Y. S., Ma, K. J., Hsu, C., Feng, S. W., Cheng, Y. C., Liao, C. C., ... Chyi, J. I. (2000). Dependence of composition fluctuation on indium content in InGaN/GaN multiple quantum wells. *Applied Physics Letters*, *77*(19), 2988-2990.

Maruska, H. P., & Tietjen, J. J. (1969). The preparation and properties of vapor-deposited single-crystal-line GaN. *Applied Physics Letters*, *15*(10), 327-329.

McNamara, D. D. (2009). *How Do Ecologites Deform in Subduction and Collision Zones?: An Alpine Study* (Doctoral dissertation, University of Liverpool). Retrieved from https:// https://core.ac.uk/reader/286187162.

Moram, M. A., & Vickers, M. E. (2009). X-ray diffraction of III-nitrides. *Reports on Progress in Physics*, *72*(3), Article#036502.

Nakamura, S., Mukai, T., & Senoh, M. (1994). High-brightness InGaN/AlGaN double-heterostructure blue-green-light-emitting diodes. *Journal of Applied Physics*, *76*(12), 8189-8191.

Ni, X., Özgür, Ü., Baski, A. A., Morkoç, H., Zhou, L., Smith, D. J., & Tran, C. A. (2007). Epitaxial lateral overgrowth of (11-22) semipolar GaN on (1-100) m-plane sapphire by metalorganic chemical vapor deposition. *Applied Physics Letters*, *90*(18), Article#182109.

Okada, N., Kurisu, A., Murakami, K., & Tadatomo, K. (2009). Growth of semipolar (1122) GaN layer by controlling anisotropic growth rates in r-plane patterned sapphire substrate. *Applied Physics Express*, *2*(9), Article#091001.

Omar, A. Z., Bakar, A. S. B. A., Makinudin, A. H. A., Khudus, M. I. M. A., Azman, A., Kamarundzaman, A., & Supangat, A. (2018). Effect of low NH3 flux towards high quality semi-polar (11-22) GaN on m-plane sapphire via MOCVD. *Superlattices and Microstructures*, *117*, 207-214.

Omar, A. Z., Shuhaimi, A., Makinudin, A. H. A., Khudus, M. I. A., & Supangat, A. (2018). Embedded AlN/GaN multi-layer for enhanced crystal quality and surface morphology of semi-polar (11-22) GaN on m-plane sapphire. *Materials Science in Semiconductor Processing*, *86*, 1-7.

Ploch, S., Frentrup, M., Wernicke, T., Pristovsek, M., Weyers, M., & Kneissl, M. (2010). Orientation control of GaN {11-22} and {10-1-3} grown on (10-10) sapphire by metal-organic vapor phase epitaxy. *Journal of Crystal Growth*, *312*(15), 2171-2174.

Ploch, S., Wernicke, T., Dinh, D. V., Pristovsek, M., & Kneissl, M. (2012). Surface diffusion and layer morphology of (11-22) GaN grown by metal-organic vapor phase epitaxy. *Journal of Applied Physics*, *111*(3), Article#033526.

Raring, J. W., Schmidt, M. C., Poblenz, C., Li, B., Chang, Y. C., Mondry, M. J., ... DenBaars, S. P. (2011). High-performance blue and green laser diodes based on nonpolar/semipolar bulk GaN substrates. *Proceedings of the International Society for Optics and Photonics 7939*, 7930. doi.org/10.1117/12.872023.

Reitmeier, Z. J., Park, J. S., Mecouch, W. J., & Davis, R. F. (2004). In situ cleaning of GaN (0001) surfaces in a metalorganic vapor phase epitaxy environment. *Journal of Vacuum Science & Technology A: Vacuum, Surfaces, and Films*, *22*(5), 2077-2082.

Rieger, W., Dimitrov, R., Brunner, D., Rohrer, E., Ambacher, O., & Stutzmann, M. (1996). Defect-related optical transitions in GaN. *Physical Review B*, *54*(24), 17596-17602.

Romanov, A. E., Young, E. C., Wu, F., Tyagi, A., Gallinat, C. S., Nakamura, S., ... Speck, J. S. (2011). Basal plane misfit dislocations and stress relaxation in III-nitride semipolar heteroepitaxy. *Journal of Applied Physics*, *109*(10), Article#103522.

Rosner, 1. S., Carr, E. C., Ludowise, M. J., Girolami, G., & Erikson, H. I. (1997). Correlation of cathodoluminescence inhomogeneity with microstructural defects in epitaxial GaN grown by metalorganic chemical-vapor deposition. *Applied Physics Letters*, *70*(4), 420-422.

Sasaki, T., & Zembutsu, S. (1987). Substrate-orientation dependence of GaN single-crystal films grown by metalorganic vapor-phase epitaxy. *Journal of Applied Physics*, *61*(7), 2533-2540.

Song, K. R., Oh, D. S., & Lee, S. N. (2013). Optical and crystal improvements of semipolar (11-22) GaN/m-sapphire by in-situ thermal etching process. *Current Applied Physics*, *13*(8), 1643-1646.

Sugahara, T., Sato, H., Hao, M., Naoi, Y., Kurai, S., Tottori, S., ... & Sakai, S. (1998). Direct evidence that dislocations are non-radiative recombination centers in GaN. *Japanese Journal of Applied Physics*, *37*(4A), L398-L400.

Sun, Q., Leung, B., Yerino, C. D., Zhang, Y., & Han, J. (2009). Improving microstructural quality of semipolar (11-22) GaN on m-plane sapphire by a two-step growth process. *Applied Physics Letters*, *95*(23), Article#231904.

Takeuchi, T., Amano, H., & Akasaki, I. (2000). Theoretical study of orientation dependence of piezoelectric effects in wurtzite strained GaInN/GaN heterostructures and quantum wells. *Japanese Journal of Applied Physics*, *39*(2R), 413-416.

Tamboli, A. C., Hirai, A., Nakamura, S., DenBaars, S. P., & Hu, E. L. (2009). Photoelectrochemical etching of p-type GaN heterostructures. *Applied Physics Letters*, *94*(15), Article#151113.

Wang, T. (2016). Topical Review: Development of overgrown semi-polar GaN for high efficiency green/yellow emission. *Semiconductor Science and Technology*, *31*(9), Article#093003.

Xu, S. R., Zhang, J. C., Cao, Y. R., Zhou, X. W., Xue, J. S., Lin, Z. Y., ... Hao, Y. (2012). Improvements in $(11\bar{2}\bar{2})$ semipolar GaN crystal quality by graded superlattices. *Thin Solid Films*, *520*(6), 1909-1912.

Yam, F. K., Low, L. L., Oh, S. A., & Hassan, Z. (2011). Gallium nitride: An overview of structural defects. *Optoelectronics-Materials and Techniques*, 4, 99-136.

Yamada, H., Iso, K., Saito, M., Masui, H., Fujito, K., DenBaars, S. P., & Nakamura, S. (2008). Compositional dependence of nonpolar m-plane InxGa1-xN/GaN light emitting diodes. *Applied Physics Express*, *1*(4), Article#041101.

Zakharov, D. N., Liliental-Weber, Z., Wagner, B., Reitmeier, Z. J., Preble, E. A., & Davis, R. F. (2005). Structural TEM study of nonpolar a-plane gallium nitride grown on (11-20) 4 H-SiC by organometallic vapor phase epitaxy. *Physical Review B*, *71*(23), Article#235334.

Zhang, Y., Bai, J., Hou, Y., Smith, R. M., Yu, X., Gong, Y., & Wang, T. (2016). Defect reduction in overgrown semi-polar (11-22) GaN on a regularly arrayed micro-rod array template. *AIP Advances*, *6*(2), Article#025201.

Zhao, G., Wang, L., Yang, S., Li, H., Wei, H., Han, D., & Wang, Z. (2016). Anisotropic structural and optical properties of semi-polar (11–22) GaN grown on m-plane sapphire using double AlN buffer layers. *Scientific Reports*, *6*(1), 1-10.

Zhao, Y., Yan, Q., Huang, C. Y., Huang, S. C., Shan Hsu, P., Tanaka, S., ... Speck, J. S. (2012). Indium incorporation and emission properties of nonpolar and semipolar InGaN quantum wells. *Applied Physics Letters*, *100*(20), Article#201108.

Zhuang, D., & Edgar, J. H. (2005). Wet etching of GaN, AlN, and SiC: A review. *Materials Science and Engineering: R: Reports*, *48*(1), 1-46.

LIST OF PUBLICATIONS AND PAPERS PRESENTED

List of Publications

1. **Anuar, A.**, Makinudin, A. H. A., Al-Zuhairi, O., Chanlek, N., Bakar, A. S. A., & Supangat, A. (2020). Growth of semi-polar (112¯ 2) GaN on m-plane sapphire via In-Situ Multiple Ammonia Treatment (I-SMAT) method. *Vacuum*, *174*, Article#109208.

2. **Anuar, A.**, Makinudin, A. H. A., Al-Zuhairi, O., Bakar, A. S. A., & Supangat, A. (2020). Crystal quality and surface structure tuning of semi-polar (11–22) GaN on m-plane sapphire via in-situ multiple ammonia treatment. *Thin Solid Films*, *697*, Article#137817.